machines

MDPI

Article

General Geometric Model for the Cutting Edge in Thread Turning

Cristian Barz [1], Oleh Onysko [2,*], Volodymyr Kopei [2], Yaroslav Kusyi [3], Lesia Shkitsa [4], Predrag Dašić [5] and Saulius Baskutis [6]

1 North University Centre of Baia Mare, Technical University of Cluj-Napoca, Victor Babes str., no.62A., 430083 Baia Mare, Romania; cristian.barz@ieec.utcluj.ro
2 Department of Computerized Mechanical Engineering, Ivano-Frankivsk National Technical University of Oil and Gas, Karpatska str., no. 15, 76019 Ivano-Frankivsk, Ukraine; volodymyr.kopey@nung.edu.ua
3 Institute of Mechanical Engineering and Transport, Lviv Polytechnic National University, 12 Stepan Bandera str., 79013 Lviv, Ukraine; yaroslav.m.kusyi@lpnu.ua
4 Institute of Engineering Mechanics and Robotics, Ivano-Frankivsk National Technical University of Oil and Gas, Karpatska str., no. 15, 76019 Ivano-Frankivsk, Ukraine; shkitsa@gmail.com
5 Engineering Academy of Serbia (IAS), Str. Kneza Miloša 9/IV, 11000 Belgrade, Serbia; dasicp58@gmail.com
6 Department of Production Engineering, Kaunas University of Technology, 56, Studentu St., 51424 Kaunas, Lithuania; saulius.baskutis@ktu.lt
* Correspondence: oleh.onysko@nung.edu.ua

Abstract

Modern requirements for highly critical threads, such as drilling tool-joint threads or trapezoidal threads of heavy machine tools, impose requirements for high accuracy and at the same time wear resistance of thread cutters. Conventional thread cutters available on the global market have a profile that coincides with the thread profile. Their rake angle and the angle of inclination of the cutting edge are typically zero. However, to ensure long tool life and high cutting performance, such tools should have optimal values of the geometric parameters of the cutting part, particularly the rake angle and the inclination angle of the cutting edge. Non-zero values of these angles distort the thread profile, and there are currently no established algorithms for profiling such cutters. This analytical study aims to develop an algorithm that enables the straightforward manufacture of high-performance and at high-precision thread cutters with interpolated straight sides profile flanks for producing trapezoidal, triangular and buttress threads, including those made of difficult-to-machine materials. The obtained analytical expressions accurately describe the cutting edge of such cutters as a hyperbola, functionally dependent on geometric parameters such as pitch, diameter and thread profile angle, as well as on the rake angle and the inclination angle of the cutting edge. To simplify manufacturing, methods of rectilinear approximation of the curvilinear profile are proposed. The validity of such a replacement has been theoretically confirmed, as the maximum deviation of the hyperbolic profile from the linear approximation does not exceed 2 micrometers. The results indicate no significant deviations in the profile angle of the cutters with relatively large rake and inclination angles ($\gamma = 10°$ and $\lambda = 7°$). Deviations from the nominal profile angle of the trapezoidal thread profile angle of 15° do not exceed 0.1°, while for tool-joint threads (30°), they range from 0.01° to 0.09°. However, significant deviations in the profile (up to 0.49°) occur in the case of machining buttress threads with a profile of 7°/45°. Experimental verification on a lathe confirms the theoretical results.

Keywords: trapezoidal thread; flank angle; rake angle; inclination angle; lead screw; buttress thread; deviation

Academic Editor: Kai Cheng

Received: 1 March 2026
Revised: 27 April 2026
Accepted: 11 May 2026
Published: 14 May 2026

1. Introduction

The modern process of research of hydrocarbon [1], geothermal [2], water [3] and soil resources [4], as well as environmental [5], recreational monitoring [6] and scientific research of subsoil and development of underground infrastructure of large cities [7] is in the focus of public attention. The key technological tool in these processes is drilled strings [8], long elastic systems with a large number of threaded connections [9], which ensure mechanical integrity and tightness of the columns in difficult well conditions [10]. Therefore, increased requirements are imposed on the strength of the connection material [11] and at the same time on its accuracy [12]. At the same time, the main advantage of threaded connections, namely the possibility of multiple assembly and disassembly, sometimes turns into a source of failures: self-unscrewing under the influence of vibration-cyclic loads [13], violation of the tightness of sealing areas [14], accelerated wear, etc. [15]. As a result, downtime, maintenance costs, and the risk of accidents increase. One of the key factors limiting the effectiveness of deep and directional drilling is uncontrolled dynamics of the drill string [16]: torsional vibrations [17], as well as axial and transverse vibrations [18]. Dynamic loads accelerate the wear of bits [19] and downhole equipment [20], worsen the operation of threaded connections [21], and affect the resource of engines and ground systems [22]. A well-known approach to solving this problem is based on the use of special vibration-proof devices [23]: drilling shock absorbers and dampers [24], elastic spindles [25], downhole motors, etc. [26]. This improves the operating modes of threaded connections, but does not eliminate the root causes of the problems. The operating environment of drill strings is characterized by abrasiveness, corrosive aggressiveness, high pressures and temperatures, as well as the action of long-term cyclic loads [27,28]. The increase in the depth and complexity of well trajectories places special demands on materials, smart structures and modern technologies for designing and manufacturing connections [29]—from the level of microgeometry to controlled residual stresses and roughness parameters [30], which determine tightness [31] and sensitivity to fatigue failure [32]. From the point of view of continuum mechanics [33], threaded profiles contain sharp-ended stress concentrators [34,35]. The stress–strain state of pipes and cylindrical shells near such concentrators in contact has been studied in detail in [35,36], which is directly relevant for the analysis of the thread root [35] and the first thread turns [36,37].

All of the above operational requirements and conditions pose the corresponding tasks of modernization of machining for manufacturers of heavily loaded threads. Therefore, a significant analysis of the machining process of parts that are mass-produced and are functionally responsible is needed. For example, the improvement of machine tools proves that it is possible to significantly increase productivity without actually losing accuracy [38], and the applied modular approach enhances optimization in the design of machine tools [39]. In addition, a significant contribution to the intensification of parts manufacturing is a scientifically based technological route, which allows for significantly optimizing the process of creating threaded parts [40,41], as well as the effective management of the life cycle of production assets [42]. However, the first priority is the modernization of cutting tools themselves: from the methods of their application to their geometric parameters [43].

2. Review of the Thread-Turning Achievements and Problems. Aim of Research

Studies on thread cutting in AISI 304L stainless steel indicate that an important argument for reducing cutter wear is the use of a combined infeed method (incremental feed) [44]. In [45], a significant increase in tool life in the process of turning a critical buttress thread from high-chromium stainless steel was proven by using a positive rake angle

of 12°. To increase the accuracy of threads, it is important to control profile deviations caused by deformations [46]. In studies [47,48], modeling the tool trajectory during thread turning, taking into account the influence of vibration, made it possible to increase the life of the cutting-edge profile. The aim of the study [49] is to increase the productivity of turning high-quality-threaded aluminum parts. To achieve this goal, the rake surface of the cutter was supplemented with micro-holes using a laser to retain solid lubricating micro- and nano-materials in them. Vector analysis predicting tangential and radial deviations of conical screw surfaces [50] shows possible ways to improve thread-turning processes. A large number of input technological parameters were taken into account in a scientific study of the surface condition of the external thread on an aviation part made of the difficult-to-machine material Inconel 718 [51]. In [52], tests of turning titanium alloy threads showed the effective effect of a cryogenic environment on reducing the amount of tool wear. The study [52] also concerned the development of a mathematical model of cutter wear to determine the expected tool life. Measurement of the profile of the resulting thread and determination of its accuracy using a special device was proposed in [53]. In contrast to measurement, in the analytical work [54], an algorithm for calculating the conical thread profile depending on the geometric parameters of a turning thread cutter with deviations is presented. The geometric three-dimensional thread-turning simulator developed on the basis of FreeCAD [55] can serve as a check or supplement to the analytical algorithm proposed in the work [54]. These results show the formation of a convex or concave thread profile instead of the expected rectilinear one. Based on the kinematics of the process of forming a conical helical surface, a method that enables the accurate formation of the screw pitch as a function of the angle of rotation of the part is proposed [56]. The study [57] presents an analysis of the movements of the cutting edge of the cutter during the process of turning a conical thread. The formation of helical linear surfaces and the accuracy of worm manufacturing are closely related to the influence of geometric parameters, including the helix angle. Therefore, approximate forms of mathematical models of helicoid accuracy are often used [58]. Measuring the accuracy of the lead screw thread pitch by the traditional method and by the method that takes into account the axial displacement of the shaft indicates a higher accuracy of the latter [59]. This is important for precision threads. The measuring and testing base of mechanical processing increasingly uses advanced thermoelectric and photovoltaic materials [60,61]. In [62], it is proposed to design a variety of cutting tools, including threaded ones, automatically using the developed surface generation method. Thread turning is a special type of cutting that requires in-depth research using systems for measuring and analyzing cutting forces [63]. Turning is always accompanied by high temperatures at the tip of the cutter. In [64], the cutting of low-alloy hardened steel in dry and minimum-lubrication conditions (MQL) was investigated. As the source [65] proves, the sizes of both the wear crater and the side wear of the cutting part directly depend on the duration of the cutting process with the insert. Therefore, the quality of the cutting insert for thread turning depends on the operating conditions: technological parameters (speed, feed, and depth), infeed methods (radial, flank, modified flank), lubrication and cooling methods and types, additional influencing factors (such as forced vibrations, cryogenic environments), as well as on the design of the tool, which takes all these factors into account. Global manufacturers of cutting tools offer carbide inserts for thread turning only with a zero rake angle (Figure 1a) [66]. However, one of the most influential factors that increase the efficiency of thread turning is the use of a non-zero rake angle of the cutter. Scientific and technical studies prove its effectiveness, especially in the manufacturing of parts from difficult-to-machine materials [44,45] (Figure 1b,c).

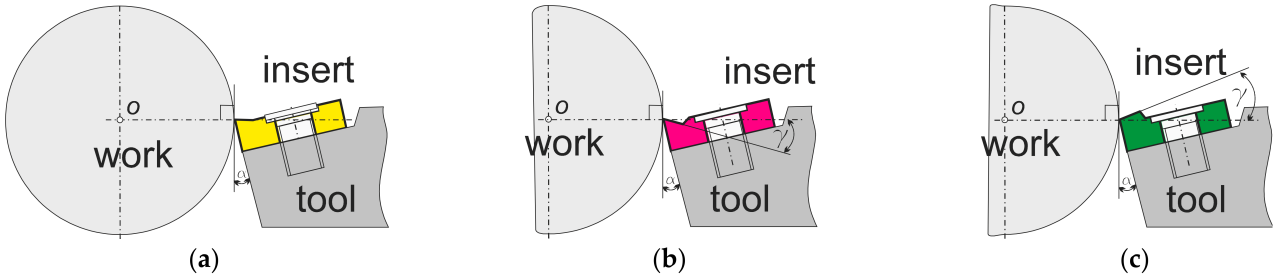

Figure 1. Diagram of the formation of geometric parameters during the turning of a part using a turning tool (α—clearance angle, γ—rake angle): (**a**) $\gamma = 0$; (**b**) $\gamma > 0$; (**c**) $\gamma < 0$.

The value of the rake angle γ, according to the original source [67], has a significant impact on the cutting forces that arise during the high-precision turning of titanium alloys. The study states that a reduced rake angle increases chip removal efficiency but accelerates tool wear. This approach provides a theoretical basis for understanding the evolution of cutting forces during thread machining of titanium alloys and serves as a guideline for tool design [67]. However, this article does not provide data on the dependence of profile accuracy or thread diameter accuracy on the rake angle, although it does include data on the dependence of surface roughness on this parameter. Despite the fact that conventional thread cutters have only zero rake angles, recommendations on appropriate rake angles values for thread turning in workpieces made of various materials are widely available in the mechanical engineering industry. Examples include works [45,67], and the study [68], which show that as the rake angle increases, the degree of chip segmentation also increases; consequently chip separation improves and the machinability increases. A high level of chip segmentation (or controlled segmentation) is desirable when machining difficult-to-machine materials such as titanium alloys and high-strength steels, as it reduces the load on the tool. The degree of chip segmentation during the machining of titanium alloys is lowest when the rake angle is in the range from 0° to 5°. At the same time, a rake angle of 15° leads to a greater degree of chip segmentation in titanium chips, and therefore improves machinability by turning [68]. There is a global practice of supplying only cutters with a zero rake angle to the market. However, it has been shown that when using standard (unadjusted) thread cutters with a rake angle different from zero, significant deviations in the pitch diameter and thread profile of the may occur [54,55]. For example, study [46] proposes inspecting the thread profile using a highly efficient contact method carried out with the cutter itself, or more precisely, with a threaded cutting insert. In this case, the measurement accuracy does not depend on whether the insert has a full or partial profile. The article indicates the deformation nature of deviations caused by the cutting forces of the cutter, whose cutting-edge profile clearly corresponds to the profile of a standard thread, and whose rake angle is 0°. According to the authors [53], a non-zero rake angle of the thread cutter is the cause of the curvilinear profile of the resulting thread. It is proposed to study the curvature of the thread profile empirically using a special device. This device makes it possible to set various cutter positions, thereby achieving specific values of the rake angle. However, the empirical approach to studying curvature cannot establish a clear functional dependence of the profile shape on the rake angle and thread parameters. Therefore, the purpose of the study is to analytically determine the profile of a carbide insert for high-precision thread turning with minimal profile deviations depending on the geometric parameters of the thread and the tool (rake angle and cutting-edge inclination angle).

The objectives of the article are as follows:

- determination of the base points of the profiles of the most common types of threads: triangular tapered, trapezoidal, and buttress, which differ significantly in the magnitude of the profile angle;
- determination of requirements for the accuracy of the profile (flank) angle of the specified threads;
- graphical study of the influence of the rake angle on the thread profile;
- application of graph-analytical and analytical methods for determining the cutting edge as the curve of intersection between the cutting-edge plane and the surface of the thread guide cone;
- development of a Python 3 program in Google Colab (https://colab.research.google.com, accessed 15 April 2026) for calculating and modeling the cutting edge of thread cutters with non-zero values of the rake angle and the cutting-edge inclination angle;
- use of the Python program for modeling cutting edges of different types of thread cutters with varying values of rake angle and cutting-edge inclination angle;
- perform an experimental verification of the results on a lathe.

3. Profile Accuracy of the Large Pitch Thread for Heavy Using Conditions

Threads with large helix angles, which are most often used in heavily loaded and critical screw pairs, can be divided into three groups according to their profile: conical threads for drill strings of a triangular profile, lead threads for kinematic pairs of a trapezoidal profile (for example, lead screws for metal-cutting machines), dynamic lead screws with a wedge-shaped buttress thread (for example, for hydraulic presses and jacks).

3.1. Profile of Conical Tool-Joint Thread According to the API and GOST Standards

Rotary drill string is a threaded drill pipe designed to transmit high torque from the ground rotor to the drill bit at the bottom of the string. In addition, a high-pressure flushing solution (up to 20 MPa) is supplied inside the string from top to bottom. An additional operational requirement is the need for multiple screwing and unscrewing of the pipes during the string lowering and lifting operations to replace a worn bit for repair. All this together imposes high requirements on the accuracy of the tool-joint conical thread, especially its profile. The strength of the connection, its tightness and unhindered multiple screwing depend on this.

According to ANSI/API standards [69] and GOST standard [70] (Figure 2), such threads are made with nominal pitches P: 4.233 mm, 5.080 mm, 6.35 mm. Diameters d_{2t} (pitch diameter) have values from 30 to 203 mm at the larger base of the cone. The thread flank angle (half-profile angle) $\varphi/2 = 30° \pm 40'$ (Figure 2).

To determine the lead angle of the thread helix, this formula is used:

$$\psi = arctan\frac{P}{\pi d_2} \quad (1)$$

Pitch P = 4.233 mm is only possible for threads of small pitch diameters of 27–41 mm. Therefore, according to the formula, the largest value $\psi = 2.86°$.

3.2. Trapezoidal Thread Profile According to ISO, ASME and GOST Standards

The main purpose of trapezoidal threads is rotational–translational kinematic pairs with significant axial loads and increased requirements for accuracy of movements. This imposes high requirements for the accuracy of the pitch and flank angle, as well as the strength and wear resistance of the lead screw and nut.

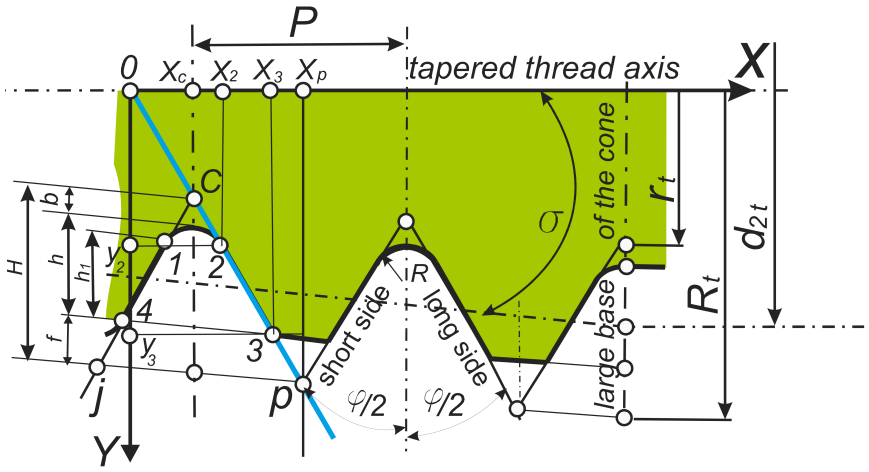

Figure 2. Scheme of a triangular conical thread according to the ANSI/API SPECIFICATION 7-2 standard [69] and GOST [70]. Parameters: φ/2—flank angle, H—height of fundamental triangle, P—pitch, h—height of the thread, h_1—height of the profile; f—truncation at the crest, b—truncation at root; R—root radius. Dimensions of the larger base of the cone: r_t—minor radius of fundamental triangle, R_t—major radius of fundamental triangle, d_{2t}—pitch diameter, σ—taper angle.

According to GOST [71], ASME [72]: $H = 1.866P$, $h_3 = 0.5P$. According to GOST [71] and ISO [73]: flank angle φ = 30°, root width $k = 0.366P$, root width along the pitch diameter is $0.5P$ (Figure 3). According to ASME [72]: root width $k = 0.3707P$, root width along the pitch diameter is also $0.5P$ (Figure 3).

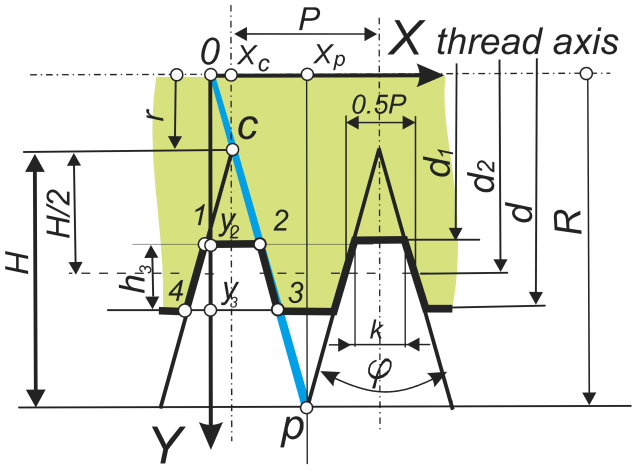

Figure 3. Trapezoidal thread diagram according to GOST 9484-81 [71], ASME [72], ISO [73], "Basic norms of interchangeability. Trapezoidal screw thread. Profiles".

The accuracy of the profile angle φ = 29° (Figure 3) of the trapezoidal thread is regulated by the ASME standard [72] and is dependent on the number of threads per inch (Table 1). That is, at Threads/In = 3 (i.e., thread pitch $P \approx 8$ mm), the accuracy of the flank angle is 22 min.

Table 1. Tolerances on φ/2 = 14.5 deg flank angle for external and internal Acme screw threads. Fragment of standard [72].

Number of Threads/In	≈Pitch	14.5 deg Variation	
	mm	deg	min
8	3.2	0	35
5	5.1	0	27

Table 1. *Cont.*

Number of Threads/In	≈Pitch	14.5 deg Variation	
	mm	deg	min
4	6.35	0	25
3	8.5	0	22
2	12.7	0	18

To determine the largest lead angle of a trapezoidal thread according to the ISO standard, one should select, according to [73], the nominal and pitch diameters of the thread of the smallest value and simultaneously with the largest pitch *P*. Table 2 contains data that can be used to determine the lead angle of the thread according to the Formula (1).

Table 2. Fragment of the ISO standard on the correspondence of maximum pitches and maximum pitch diameters [73].

Major Diameter *d*, mm	Pitch *P* (Maximum), mm	Pitch Diameter (Maximum), mm	Lead Angle, ° ψ
16	4	14.00	5.2
24	8	20.00	7.26
32	10	27.00	6.72
44	12	38.00	5.7

Therefore, according to the Formula (1), the largest lead angle in a trapezoidal thread with a major diameter of 24 mm and a pitch 8 mm is 7.26°.

3.3. Buttress Thread Profile According to the ASME Standard

The main purpose of buttress threads is to withstand high axial loads in one direction, for example, industrial jacks, casing pipes for oil and gas wells with significant axial loads and increased requirements for accuracy of movements, which imposes high requirements for the accuracy of the pitch and flank angle, as well as the strength and wear resistance of the screw and nut (Figure 4).

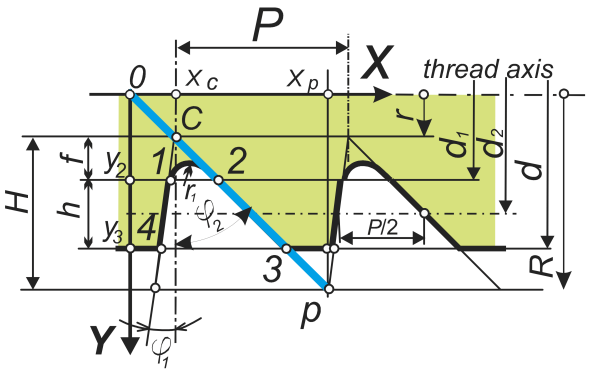

Figure 4. Buttress thread pattern according to ANSI standard [74]. Symbols: d—major diameter, d_1—minor diameter, d_2—pitch diameter, P—pitch, H—height of sharp-V thread, h—basic height of thread engagement, r_1—root radius (theoretical), f—crest truncation, F—crest width.

Tolerance of the thread profile angle according to the ANSI B1.9–1973 standard [74]: $H = 0.89064P$, $h = 0.6P$, $r_1 = 0.07141P$, $f = 0.14532P$, $F = 0.16316P$, $\varphi_2 = 45°$, $\varphi_1 = 7°$.

The accuracy of the flank angles of the thread according to the ANSI standard [74] is represented by the tolerances for angle deviation: 4 min for $\varphi_2 = 45°$ and 5 min for $\varphi_1 = 7°$ (Table 3).

Table 3. Fragment of the ANSI standard on major diameters, pitch and flank angle accuracy [74].

Threads per Inch	Pitch, *P*, ≈mm	Tolerance on Flank Angles of Thread, ±min		Pitch Diameter d_2, Inch
		$\varphi_1 = 7^\circ$	$\varphi_2 = 45^\circ$	
16	1.6	5	4	0.5–4
10	2.5	5	4	0.3–16
4	6.35	5	4	1.5–24
2	12.7	5	4	8–24

Therefore, according to the Formula (1), the largest lead angle in the buttress thread with a pitch diameter of 1.5′ ($d_2 \approx 38$ mm) and a pitch of $P \approx 6.35$ mm is $\psi = 3.03^\circ$.

3.4. Comparison of Requirements for the Accuracy of the Thread Profile Angle and the Lead Angle

So, nominally the most demanding in terms of accuracy of flank angles is the buttress thread according to the standard [73] with a deviation of 4 min, which is $\delta = 4/(45 \times 60) = 0.15\%$ of the nominal value (Table 4). The trapezoidal thread according to the ASME standard [71] with a deviation of 18 min can be considered less accurate, i.e., $\delta = 18/(60 \times 14.5) = 2\%$. The least demanding profile accuracy is the tool-joint thread with a deviation of 45 min, which is $\delta = 45/(60 \times 30) = 2.5\%$ of the nominal value of the profile angle (Figure 2).

Table 4. Summary of maximum data for buttress, trapezoidal and tool-joint threads in terms of profile angle deviation and lead angle.

Parameters	Tool-Joint	Trapezoidal	Buttress
Maximum permissible relative deviation of the profile angle δ	2.5%	2%	0.15%
Maximum thread lead angle ψ (maximum helix lead angle)	2.86°	7.26°	3.83°

It should be noted that buttress threads ($P = 5.08$ mm) as well as triangular tapered threads ($P = 3.175$ mm) are also widely used in the oil and gas industry, for example, for connections of well casing pipes. However, despite the high mechanical loads and requirements for corrosion resistance, these threads have quite large diameters (114–508 mm) and therefore, with similar pitch values [75], have a significantly lower lead angle than those used in highly loaded threads [76], for example in powerful jacks.

4. Modern Approaches to Ensuring the Accuracy Form of the Production of Large-Step Threads Made by Turning

4.1. Providing Directrix and Generatrix Lines When Turning Helical Surfaces

All modern threads contain two helical surfaces, with a constant pitch *P*. Figures 2–4 show a blue line *cp*, which is the directrix of one of these two helical surfaces. Points 2 and 3 belong to this directrix and are at the same time profile points of the threads: tool-joint, trapezoidal, buttress. Other profile points of these threads 1 and 4 belong to the generatrix of the second helical surface. Since lathes are widely used to manufacture the specified threaded and helical surfaces, considerable attention of manufacturers and researchers is focused on thread cutters and their ability to process difficult-to-machine materials, which include high-strength and corrosion-resistant steels [77]. Of course, such abilities are developed due to the use of modern composite materials for coatings of cutting threaded inserts [78]. At the same time, the actual geometric parameters of the cutters and their movements during thread turning are very influential factors, especially for difficult-to-machine materials [45].

Usually, in the case of threading on a lathe, the cutter is installed in such a way that its cutting edge 4-1-2-3 is aligned with the axial plane of the thread [66,76] (Figure 5). Each

point of the cutting edge performs an absolute movement along the trajectory of the helix with a pitch P. Points 2 and 3 belong to one helical surface and two boundary helices of this surface: the blue helix with the smallest radius r_2 (point 2) and the red helix with the largest radius R_3 (point 3). All other points forming the helical surface are located between the points 2 and 3. Another helical surface is formed by the section of the cutting edge located between the points 1 and 4. The absolute movement of the edge points along the helix is ensured by the constant rotational movement of the workpiece around the thread axis X and the translational movement of the cutting edge points along the axis X. In this case, the module of translational movement $\left|\vec{S_t}\right|$ (mm per rotate) is equal to the step size P (mm).

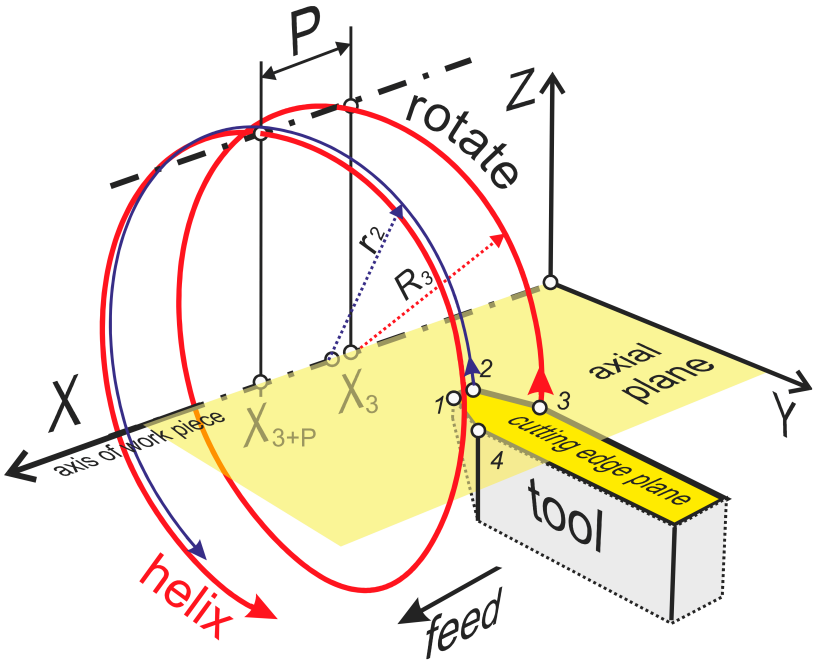

Figure 5. Thread cutter movement diagram: X—axis, P—pitch, S_t—longitudinal feed per revolution, R_3—radius of the helix (red) with point *3* on the cutting edge, r_2—radius of the helix (blue) with point *2* on the cutting edge, X_3,X_{3+P}—coordinates of the points of two adjacent turns of the red helix on the X axis; 4, 1, 2, 3 are points that simultaneously belong to the cutting edge of the cutter and the axial plane of the screw XY (yellow).

Provided that the plane of the cutting edge of the tool is completely aligned with the axial plane of the thread, profiles of the edge and the thread will coincide, and accordingly their profile angles φ will coincide (Figure 6a).

Theoretically, the helical surface is formed by a truncated cone (guide cone), which rotates with a constant circular speed around its axis X and moves translationally along this axis. If the cutting edge 3-2 of the cutter lies in the axial plane of the guide cone—the plane X_p-X_c -*c*-*p*, then a regular closed cone is formed in the case of radial feed $\vec{S_r}$ (Figure 6c). The straight-line generator of the cone *pc* will coincide with the edges 2-3 when the cutter completes the radial feed $\vec{S_r}$. Such a guide cone provides a theoretically correct closed helicoid (otherwise Archimedes' screw), which defines most fastening threads and all buttress threads and trapezoidal lead screws (Figure 6b). The profile of the guide cone is the same in all axial planes, including ZX. The directrix *cp* in the ZX plane is described by the equation (Figure 6d):

$$z = x \cdot \cot\left(\frac{\varphi}{2}\right)$$

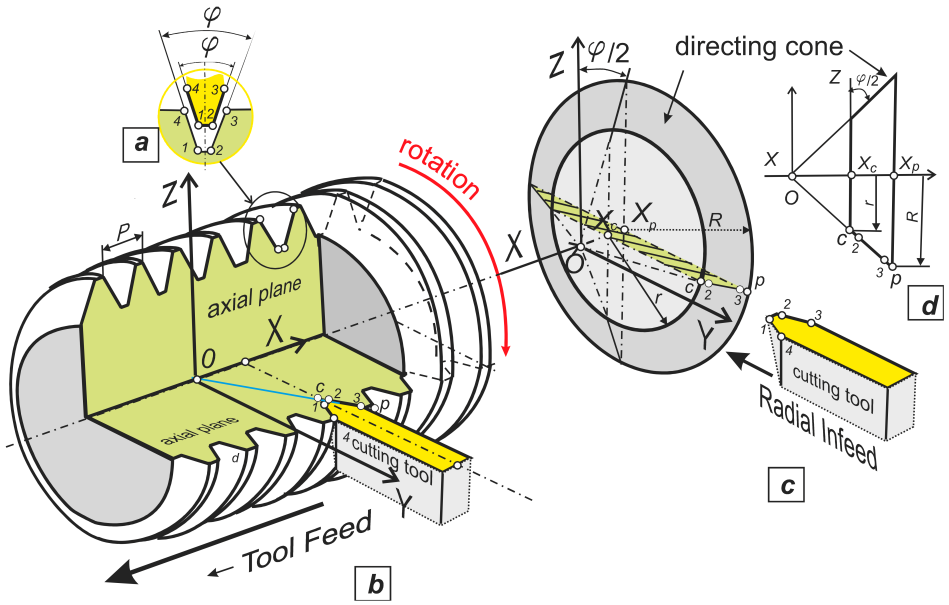

Figure 6. Scheme of forming a trapezoidal thread: (**a**)—coincidence of the cutting-edge profile (yellow) and the profile of the resulting thread (lime); (**b**)—location of the edge of the thread cutter (yellow) in the axial plane of the thread (lime); (**c**)—location of the edge of the cutters 2-3 as the generator of the guide cone *cp*. *X*—thread axis, *P*—thread pitch, *R*—radius of the larger base of the guide cone, *r*—radius of the smaller base of the guide cone, X_p, X_c—coordinates of the points of the generating cone of the directrix on the thread axis *X*; φ—thread profile angle; (**d**)—location of the projection of the cutting edge 2-3 in the axial plane *ZX*.

4.2. Deviation of the Cutting Edge of the Thread Cutter from the Generating Helical Surface Under the Condition of Using the Cutting-Edge Inclination Angle λ

In practice, leading manufacturers of cutting tools often recommend using a special inclination of the cutting insert at an angle λ to the thread axis and supply special shims for this. This inclination angle λ, which is equal to the lead angle, guarantees the same clearance angles of the right and left sides of the insert [66,76] (Figure 7a). This is done to maintain the same operating conditions of the left (1-4) and right (2-3) cutting edges, which helps to increase the tool life. For versatility, the cutting-edge profile of such carbide inserts 4-1-2-3 is made identical to the profile of the corresponding thread (Figure 7b). The diagram of installing the cutter together with the holder with a rotation to an angle λ (Figure 7c) graphically explains the difference compared to installation without rotation to this angle (Figure 6b). However, such an installation is not possible in a conventional lathe toolholder.

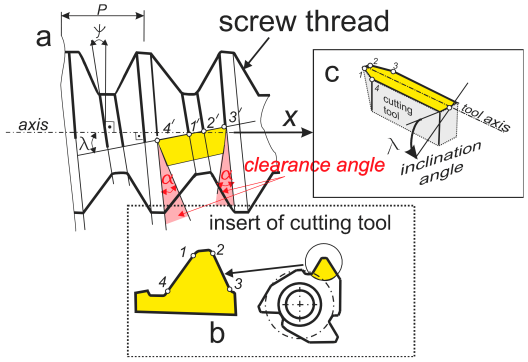

Figure 7. Scheme of installing the cutting insert of the thread cutter: (**a**) at the angle of inclination of the edge λ which corresponds to the lead angle ψ; (**b**) placement of the cutting edge on the threaded insert; (**c**) scheme of turning the thread cutter at an angle λ.

However, it is obvious that the plane where the cutting edge 2-3 is located, in the case of its inclination at an angle λ to the axial plane of the thread (Figure 8a), will not coincide with the generator of the guide cone *cp*. (Figure 7c), which is always located in the axial plane (lime) (Figure 8b).

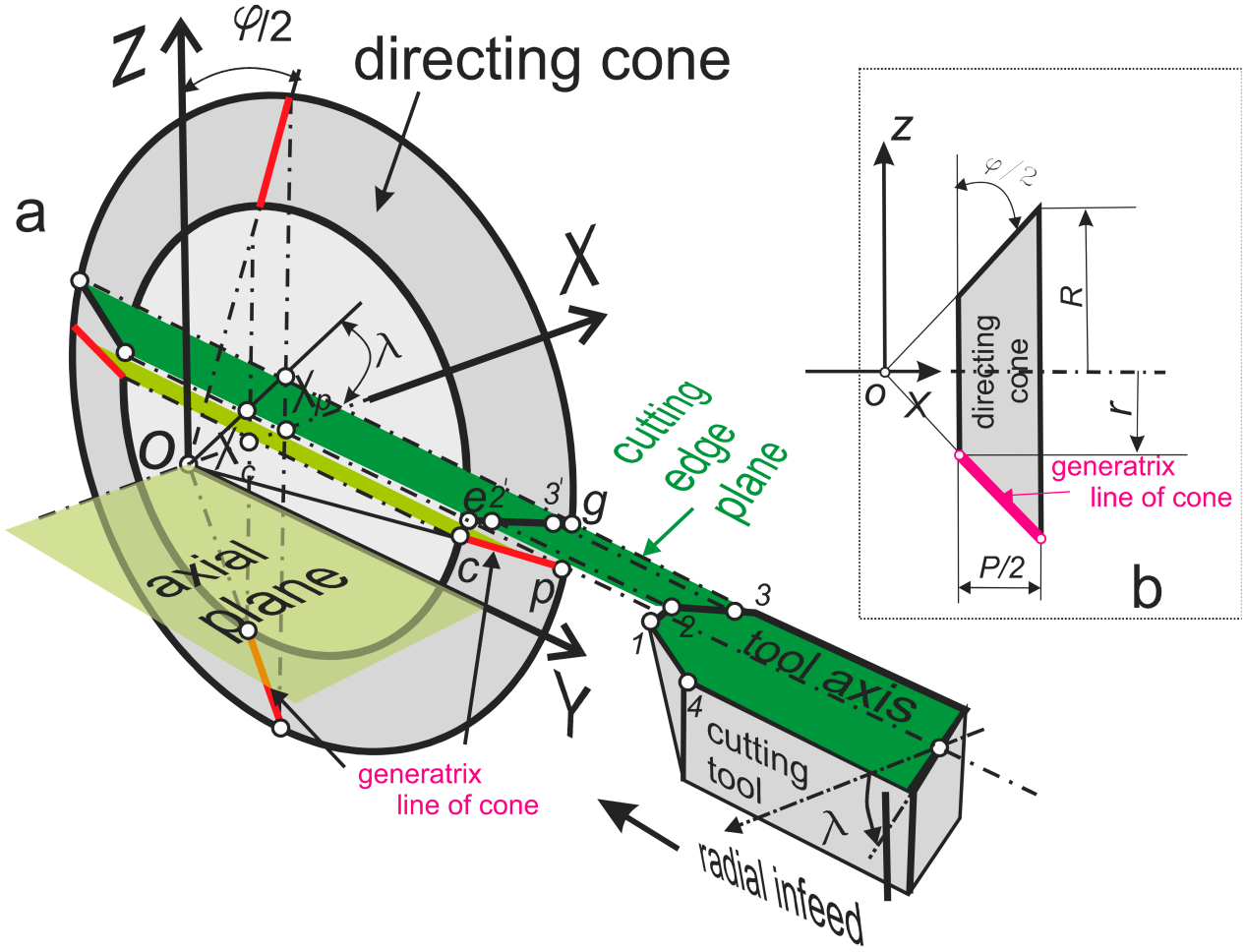

Figure 8. Scheme of installation of the cutting insert of the thread cutter: (**a**) at the angle of inclination of the edge λ, which corresponds to the lead angle ψ; (**b**) axial projection of the guide cone; *P* is the thread pitch, φ is the profile angle of the thread. Radii *r* and *R* are the parameters of the large and small base of the truncated cone (guide cone).

4.3. Deviation of the Cutting Edge of the Thread Cutter from the Generating Helical Surface Under the Condition of Using the Rake Angle γ

If the value of the rake static angle at the apex of the thread cutter is not zero, but the angle of inclination of the cutting edge has a zero value, then the rake plane intersects the generating cone of the thread parallel to its axial plane (Figure 9). The value *k* is the distance from the plane of the section of the guide cone with the plane of the cutting edge of the cutter 2-3-4-1 to the axial plane. *eg* is the line of intersection of the plane of the cutting edge with the guide cone. Obviously, the curve *eg* is not equal to the line *cp*, but it represents the true generator of the guide cone and must include the cutting-edge points located between the points 2 and 3 (Figure 9).

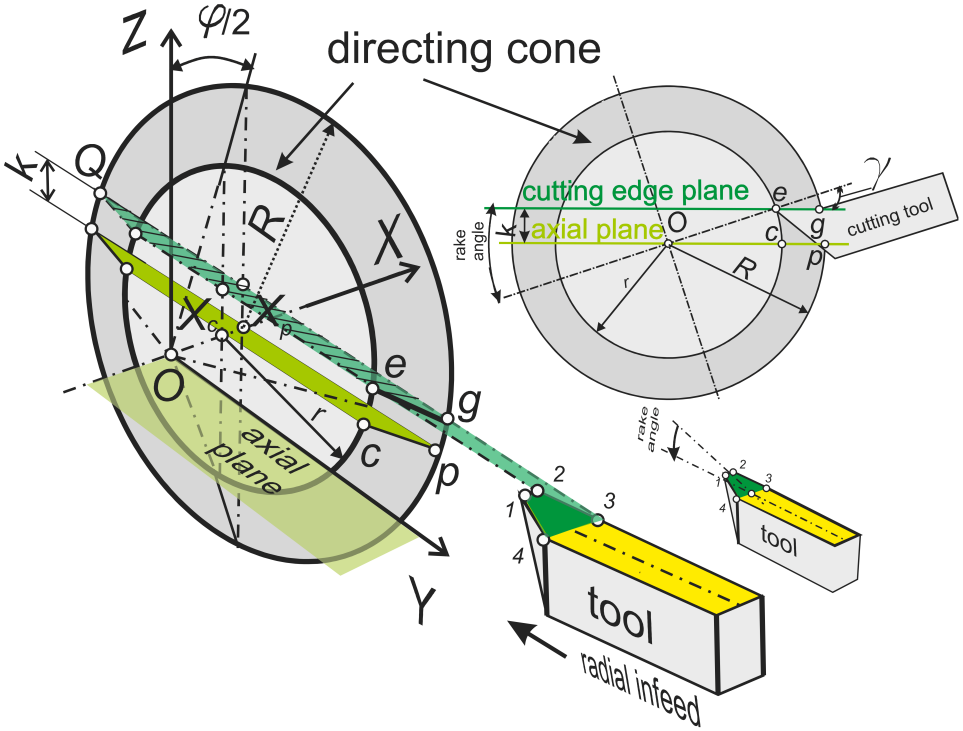

Figure 9. Installation diagram of a thread cutter with a non-zero rake angle, *Spop*—transverse feed.

5. Analytical Calculation of the Points of the Hyperbolic Profile of the Cutting Edge with a Non-Zero Value of the Rake Angle and the Inclination Angle at the Nose

5.1. Analytical Calculation of the Hyperbolic Profile of the Cutting Edge as a Function of the Rake Angle

In fact, when a conical surface is intersected by a plane parallel to the axis of the cone, a hyperbola is formed [79,80]. So, Figure 10 presents a spatial scheme for the formation of a hyperbolic curve *ge*, which should be in the shape of the cutting edge of the cutter to create one of the two helical surfaces of the thread with a pitch *P*, a profile angle of the thread φ and the height of the initial triangle *H*.

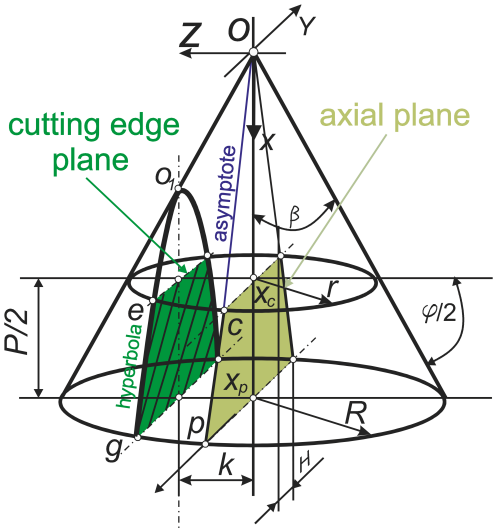

Figure 10. Scheme of obtaining a cross-section of a conical surface and a plane parallel to the axis of the cone. The Y-axis is parallel-transferred from the vertex of the cone O to the point Xp and then through the point p.

Therefore, the shaded area in the figures corresponds to the hyperbolic section of the rake plane with the surface of a truncated cone, which is the parallelism surface of a triangular, trapezoidal, or buttress thread [81].

The axes x_2 and x_1 lie, respectively, in the planes of the major and minor bases of the truncated cone.

If the cutting edge is not located in the axial plane of the truncated cone, which is given by the trace f_β (Figure 11), passing through the thread axis, then a cutter with a triangular profile, which should correspond to the thread profile during transverse feed, will reproduce not a triangular, but a hyperbolic thread profile [78].

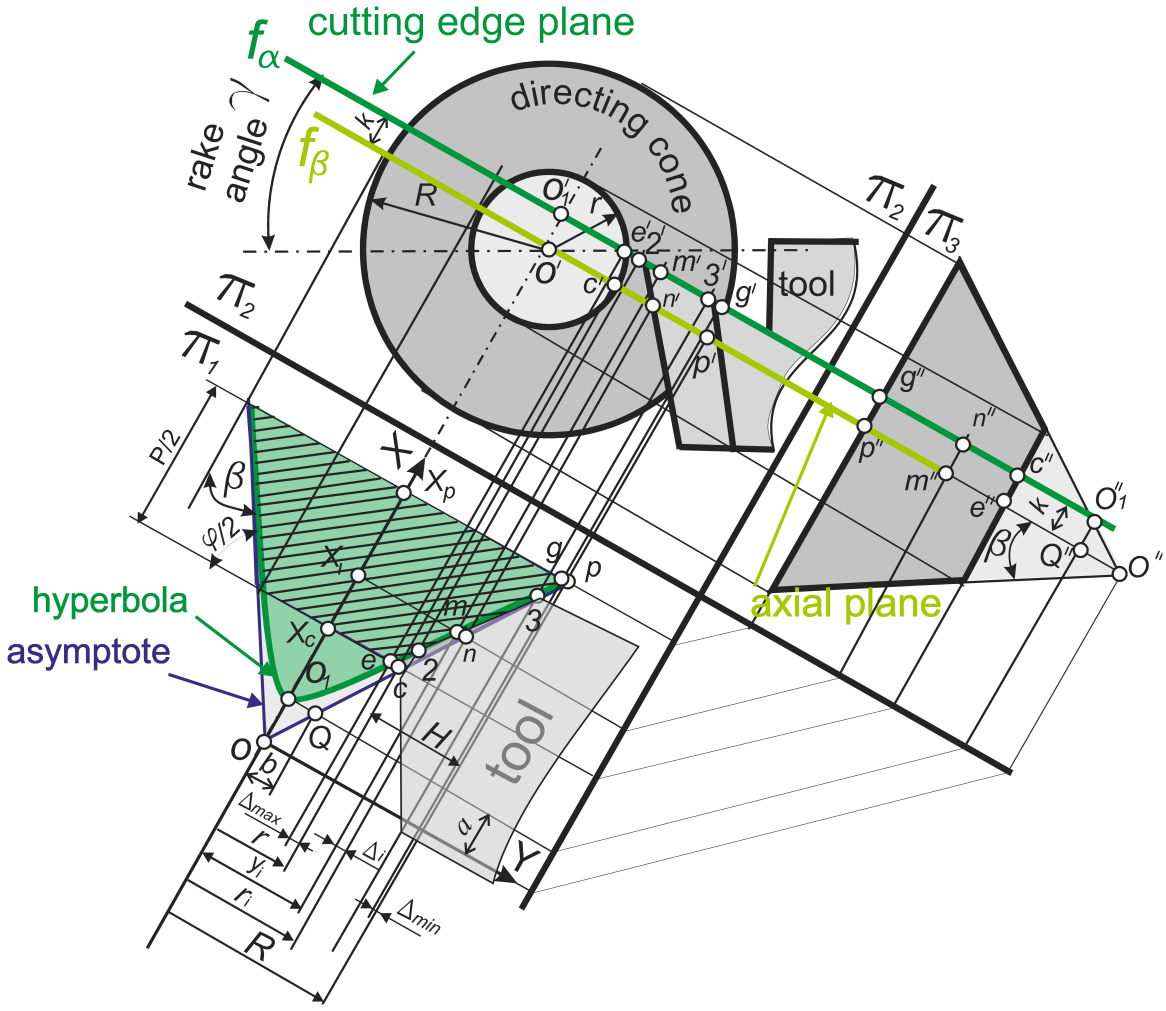

Figure 11. A complex drawing of obtaining a cross-section with a hyperbolic profile when intersecting a cone with a plane that does not pass through its axis.

Therefore, if we consider the section of the thread as the surface of a truncated cone (Figures 10 and 11) with a large radius R, a small radius r and an angle at the nose, then as a result of the intersection of this cone with the rake plane, which is given by the trace f, a hyperbola will be obtained [80].

Hyperbolic section of a cone with axis OX and generatrix Or with the rake plane marked by the shaded area (Figure 11). Hyperbola O_1 *emq* asymptotically approaches the line Op. An arbitrarily chosen point m at the intersection of the axial plane and the cone corresponds to a point n at the intersection of the rake plane and the cone. They have a common coordinate x_n on the OX axis. The vertex O_1 of the hyperbola is distant from the

vertex of the cone by a distance a along the OX axis, and the point Q is distant by a distance b along the OY axis.

To calculate the deviation of the hyperbola from the asymptote, depending on the distance from the vertex of the cone O along its axis, we use the following formula [80]

$$|mn| = \frac{ab}{x_n + \sqrt{x_n{}^2 - a^2}} \tag{2}$$

We obtain the dependence of the value of a on the values of the angles β and γ and the radius r. To do this, we determine the value of k, which is marked on the projection plane W (Figure 11). From the right triangle $O''O_1$ "Q":

$$k = |O''Q''|tan\beta$$

Using the projection plane H, we obtain the expression

$$k = a{\cdot}tan\beta$$

Since the value k is equal to the length of the segment $O_1{}'O'$ on the projection plane V (Figure 11), then from the right triangle $O_1{}'O'e$ we have the equation

$$\left|O_1'O'\right| = k = \left|O_1'e\right|sin\gamma = rsin\gamma$$

Therefore:

$$k = rsin\gamma \tag{3}$$

and accordingly, since $|Q_1{}'O'| = |Q_1{}''O'| = k = r\sin\gamma$:

$$a = \frac{r{\cdot}\sin\gamma}{\tan\beta};$$

From the same constructions, we obtain the dependence

$$b = a{\cdot}\tan\beta = r{\cdot}\sin\gamma$$

As a result, we obtain the dependence of the product ab on the values of the angles β and γ and the radius r:

$$ab = \frac{(r{\cdot}\sin\gamma)^2}{\tan\beta} \tag{4}$$

Since point n is taken as an arbitrary point of the cone, and point m is the corresponding point of the hyperbola, then using the concept of an arbitrary i-th point, we will take its coordinates as x_i along the OX axis and r_i along the OY axis. Thus, the asymptote formula will look like this:

$$x_i = \frac{r_i}{\tan\beta} = \frac{r_i}{\tan\left(\frac{\pi}{2} - \frac{\varphi}{2}\right)} = \frac{r_i}{\cot\frac{\varphi}{2}} \tag{5}$$

We replace the notations: $|mn|$ by Δ_i, as well as x_n by x_i and after substituting expressions (4) and (5) into Formula (2), we obtain the formula

$$\Delta_i = \frac{(r{\cdot}\sin\gamma)^2/\tan\beta}{\frac{r_i}{\tan\beta} + \sqrt{\left(\frac{r_i}{\tan\beta}\right)^2 - \left(\frac{r{\cdot}\sin\gamma}{\tan\beta}\right)^2}} = \frac{r^2{\cdot}\sin^2\gamma}{r_i + \sqrt{r_i{}^2 - (r{\cdot}\sin\gamma)^2}} \tag{6}$$

The obtained Equation (6) indicates the functional dependence of the magnitude of the displacement of Δ_i the hyperbolic profile of the cutting edge of the thread cutter at an arbitrary i-point on the value of the rake static angle γ at the vertex point e and the radius of the cone at an arbitrary point r_i and the small radius r of the truncated cone.

An arbitrary point on the hyperbola profile can be given in parametric form:

$$y_i = r_i - \Delta_i$$

$$x_i = \frac{r_i}{\cot\frac{\varphi}{2}}$$

So, we describe the profile of the hyperbola as follows:

$$y_i = x_i \cdot \cot\left(\frac{\varphi}{2}\right) - \frac{r^2 \cdot \sin^2\gamma}{x_i \cdot \cot\left(\frac{\varphi}{2}\right) + \sqrt{\left(x_i \cdot \cot\left(\frac{\varphi}{2}\right)\right)^2 - (r \cdot \sin\gamma)^2}} \quad (7)$$

where:

r_i—thread radius at a given point of the profile,
x_i—coordinates of the thread profile (2–3) or (1–4) in Figure 3,
φ—profile angle of the thread.

5.2. Implementation of Formulas (1)–(7) in Python Using the Example of Analyzing the Process of Turning a Trapezoidal Thread of Diameter 24 mm with a Pitch of 8 mm Using a Cutter with a Rake Angle of $\gamma = 50°$

The obtained hyperbola functions (Equation (7)) and asymptotes make it possible to make their graphical display and graph-analytical comparison. Figure 12 presents the diagrams of the specified functions made by the authors in Python [82], as well as the diagram of linear interpolation of the hyperbola by the two extreme points *e* and *g*. Only in order to clearly distinguish visually between the hyperbola and its asymptote, the value of the rake angle $\gamma = 50°$ was used. For example, the diagrams (in Figure 12) were simulated based on the data of the trapezoidal thread according to ISO 2904 and GOST9484-81 with a nominal diameter of 24 mm and a pitch of 8 mm (Figure 3). The diagram in Figure 12, for the sake of clarity of its perception, has been copied into Figure 13, where it is commented on with data and terms from Figures 10 and 11.

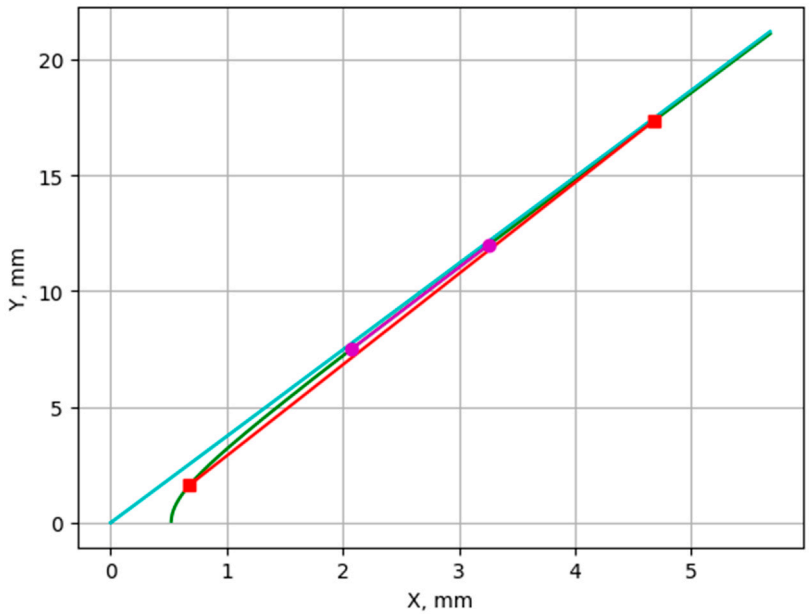

Figure 12. Diagram of the straight section of the trapezoidal thread profile according to ISO 2904/GOST9484-81 with a nominal diameter of 24 mm, a pitch of 8 mm (blue line), a hyperbolic profile of the cutting edge of the cutter as a function of the rake angle $\gamma = 50°$ (green curve), and a linear interpolation of the hyperbola by the two points (red line, magenta line).

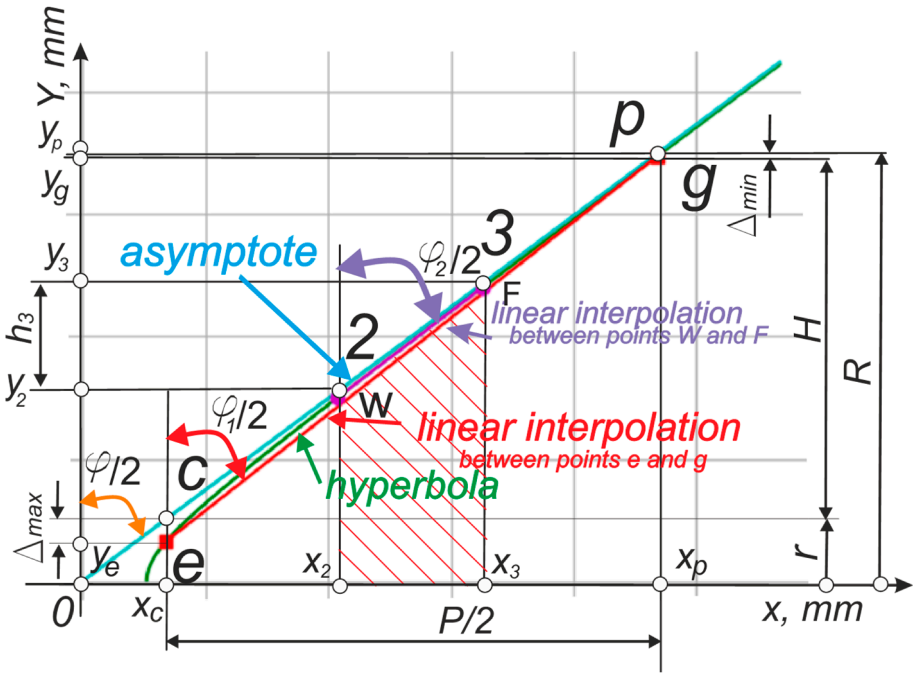

Figure 13. Diagrams with comments: straight-sided section of the profile of a trapezoidal threads 2-3 according to ISO 2904 [73] and GOST 9484-81 [71], with a nominal diameter of 24, a pitch of 8 mm (orange straight line) and a hyperbolic profile of the cutting edge of the cutter as a function of the rake angle $\gamma = 50^\circ$ (section on the blue curve between points with coordinates x_2 and x_3).

5.3. Analysis of the Convexity (Concavity) Arrow of a Hyperbola and Its Maximum and Minimum Deviations from the Asymptote

Visual scaling of the thread profile and cutting edge of the thread cutter in Figure 14 was performed to determine:

The values of the maximum Δmax and minimum Δmin deviations of the simulated hyperbolic curve (green) *emg* (which includes the model of the cutting-edge profile of the thread cutter) from the asymptote *cp* (the given cutting-edge profile, which is equal to the profile of the given thread (dotted cyan)).

Interpolation line through two points *W* and *F*, which lie on the hyperbola *emg* and are defining points 2 and 3 of the simulated cutting edge of the thread.

The angles of the standard cutting-edge profile (φ/2) (Figures 13 and 14a) and the angle of the interpolation line *eg* (red) ($\varphi_1/2$) (Figures 13 and 14a).

Concavity values $|Am| = si$ of the points *m* of the obtained hyperbolic profile of the cutting edge of the thread cutter *emg* from points *A* on the interpolation line *eg*.

Profile angle $\varphi_2/2$ of the simulated cutting edge (*WF*) intended for forming the straight-sided section of the thread profiles 2–3, which belongs to the asymptote (Figures 13 and 14b).

5.3.1. The Formulas for Calculating the Maximum Deviations Δmax and Minimum Deviations Δmin

Deviations of the simulated hyperbolic curve *emg* (which includes the model of the cutting-edge profile) from the asymptote *cp* (a given cutting-edge profile equal to the profile of the given thread) can be determined based on the Formula (6):

$$\Delta_i = \frac{r^2 \cdot \sin^2 \gamma}{r_i + \sqrt{r_i^2 - (r \cdot \sin \gamma)^2}}$$

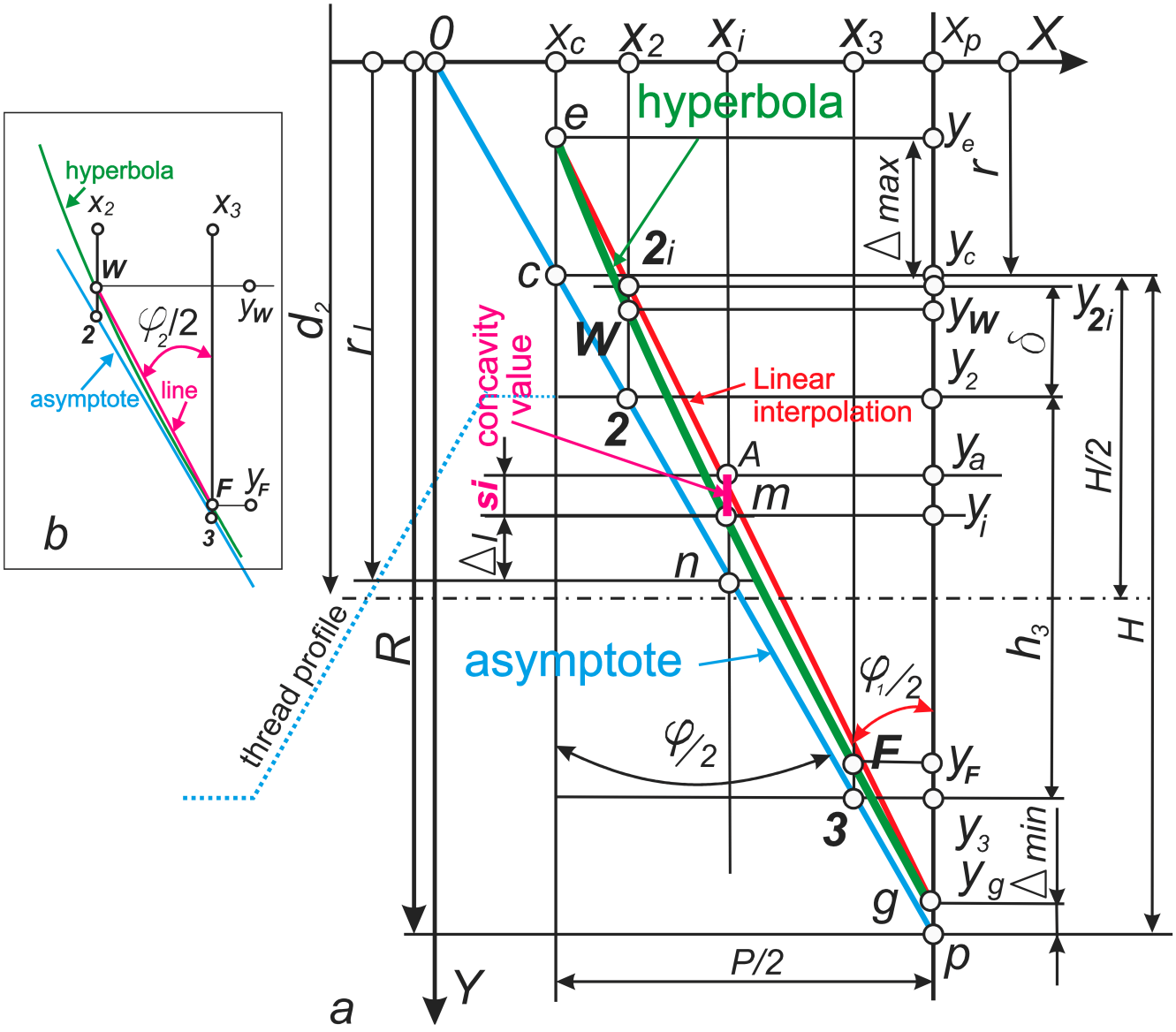

Figure 14. Scheme for determining the hyperbolic curve *emg* and: (**a**) the convexity arrow s_i of an arbitrary point *n* of the hyperbolic curve *emg*; (**b**) the profile angle $\varphi_2/2$ of the simulated cutting edge (*WF*) intended for forming the straight-sided section of the thread profile 2–3, which belongs to the asymptote *cp* of the hyperbolic curve *emg*.

According to Figures 11 and 14, to determine Δmax, the following substitution should be made $r_i = r$:

$$\Delta_{max} = \frac{r^2 \cdot \sin^2 \gamma}{r + \sqrt{(r)^2 - (r \cdot \sin \gamma)^2}} = r - \frac{r \cdot \sin^2 \gamma}{1 + cos\gamma} \quad (8)$$

According to Figures 11 and 14, to determine Δmin, the substitution should be made $r_i = R$:

$$\Delta_{min} = R - \frac{r^2 \cdot \sin^2 \gamma}{R + \sqrt{R^2 - (r \cdot \sin \gamma)^2}} \quad (9)$$

5.3.2. Determination of the Angles of the Interpolation Lines eg and wf

Proflie angles $\frac{\varphi}{2}$, $\frac{\varphi 1}{2}$, φ2/2 can be determined by Figure 14 and formulas in Table 5:

Table 5. Summary of angle calculation formulas φ, φ_1, φ_2.

Symbol	Name	Formula	Comments
φ/2	Flank angle (half-profile angle)	$\frac{\varphi}{2} = arctan\frac{x_3-x_2}{y_3-y_2}$	15° according to standards ISO 2904 [73] and GOST 9484-81 [71]
$\varphi_1/2$	The angle of the interpolation line between points g and e	$\frac{\varphi_1}{2} = arctan\frac{x_p-x_c}{y_g-y_e}$	$x_c = r\tan\frac{\varphi}{2}$ $x_p = R\tan\frac{\varphi}{2}$ $y_c = r$ $y_e = r - \Delta_{max}$ $y_p = R$ $y_g = R - \Delta_{min}$
$\varphi_2/2$	Cutting-edge profile angle	$\frac{\varphi_2}{2} = arctan\frac{x_3-x_2}{y_F-y_w}$	$x_3 = \left(r + \frac{H}{2} + \frac{h_3}{2}\right)\tan\frac{\varphi}{2}$ $x_2 = \left(r + \frac{H}{2} - \frac{h_3}{2}\right)\tan\frac{\varphi}{2}$ y_f determined by *(7)* for $x_i = x_3$ y_w B determined by *(7)* for $x_i = x_2$

5.3.3. Definition of the Deviation (Concavity Value) of Hyperbola *emg* by Software-Analytical Method

For the analytical definition of the deviation (concavity value) of the hyperbola *emg*, it is necessary to find the maximum distance between the points of the hyperbola and the corresponding points of the interpolation line $|Am| = si$. (Figure 14), that is, find the maximum value of the difference between Y coordinates:

$$|s_i| = y_{int} - y$$

where

y is determined by Formula (7) for a given array of points with coordinates x_i for $i = \{x_c, \ldots x_p\}$;

y_{int}—for the same array of points $i = \{x_c, \ldots x_p\}$, using Figure 14 we determine using the method [80] the interpolation line *eg*, i.e., we create a line through the point $e(x_c, y_e)$.

5.3.4. Maximum Possible Distance si

Based on the algorithm built on the basis of Formula (7), a Python application [82] was created to determine the maximum possible distance si (Table 6).

Table 6. Data and results of the calculation of the boom s_i convexity of hyperbola *emg*.

Thread Diameter, mm	Thread Pitch	The Value of the Rake Angle γ, °	si, mm
24	8	50	0.01
24	8	20	0.002
24	8	10	0.00056

5.3.5. Definition of the Arrow of Convexity (Concavity Value) of the Hyperbola Section emg, Which Corresponds to the Cutting Edge of WF by the Program in Python

Based on Figure 14 and using the Python, an application [82] was developed that allows calculating the distances between the hyperbola and the straight interpolation line drawn through the points W, F of the cutting edge of the modeled cutter for machining the threaded parts 2–3. The program allows for a rectilinear approximation of the hyperbola section *emg*.

Figure 15 shows the distribution graphs of these distances: between the hyperbola and the interpolation line *WF* (upper curves), between the hyperbola and the approximation line (lower curves).

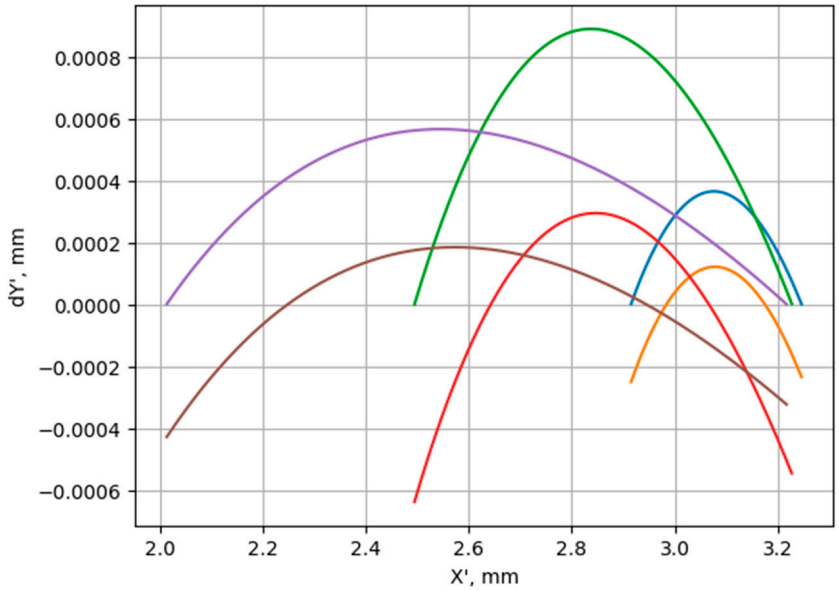

Figure 15. Distances from the interpolation line *WF* (upper curves) and the approximation line (lower curves) to the corresponding points of the hyperbolic curve *WF* modeled according to the Formula (7) intended for forming the cutting edge *2–3* of a tool with a rake angle γ = 10° for *P* = 2 mm (right), 5 mm (middle), 8 mm (left).

Thus, it is shown that, due to the small concavity value, it is technologically expedient to manufacture the cutting edge with a rectilinear rather than hyperbolic profile of the lateral side flanks.

6. Analytical Calculation of Linear Interpolation Between Two Extreme Points of the Hyperbolic Cutting-Edge Profile as a Function of the Rake Angle at the Nose and the Inclination Angle

To ensure high productivity of the thread cutter, the cutting edge plane (i.e., the rake plane) should be placed not only at the rake angle γ, but also at the cutting-edge inclination angle λ, as recommended by tool manufacturers [66,76].

From the point of view of the well-known theory of conic sections [80], a hyperbola will be obtained under the conditions:

- if we cross the conical surface with a plane that is parallel to the axis of the cone. In Figure 16a, the plane *f* intersects the conical surface at a distance *k* from the axis and is located parallel to the axis. The value of *k* depends on the value of the rake angle according to the Formula (3);
- if we cross the conical surface at an angle λ whose value is greater than 0° and less than the angle at the vertex of the cone β (Figure 16b);
- if we cross the conical surface with a plane parallel to the generator of the cone, we will obtain a parabolic profile (Figure 16c).

That is, provided that $0^\circ < \lambda < \left(\frac{\pi}{2} - \frac{\varphi}{2}\right)^\circ$ the cross-section of this triangular thread and the plane of the rake surface with a double slope is hyperbolic.

It is possible to determine the coordinates of the extreme points of the intersection of the plane *uAv* with the surface of a truncated cone with height $\pi/2$ as the lines of intersection of the hyperbola with circles with radii *r* and *R* (Figure 17).

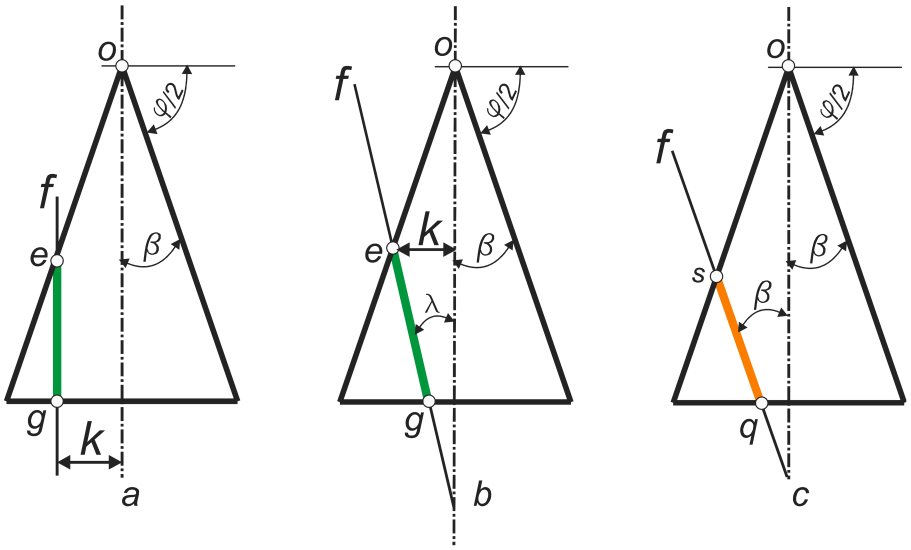

Figure 16. Schemes illustrating the origin of the hyperbolic and parabolic cross-section depending on the position of the rake plane (**a**): f—frontal trace of the rake plane (**b**), λ—inclination angle of the rake plane to the axis of the conical surface (**c**), β—half angle at the apex of the cone.

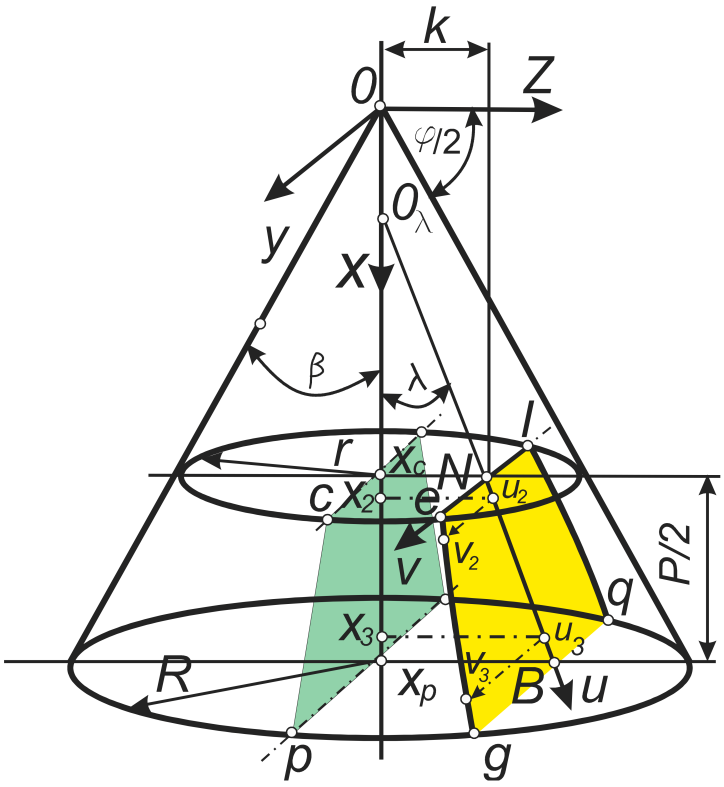

Figure 17. Scheme for obtaining a cross-section of a conical surface and a plane uNv inclined to the axis of the cone at an angle λ.

Therefore, the indicated shaded region is bounded by a hyperbolic curve formed by the intersection of the rake flat surface of the thread cutter, whose parameters $\lambda \neq 0$ and $\gamma \neq 0$ the parallelogram surface of the triangular thread, i.e., with a cone of height h and an angle at the vertex β.

It is possible to determine the coordinates of the extreme points of the intersection of the plane uNv with the surface of a truncated cone with height $\pi/2$ as the lines of the intersection of a hyperbola with circles of radii r and R (Figure 17).

In the plane of a circle with radius r (plane $y0x_2$)—coordinates on the v axis:

$$v_{min} = \sqrt{r^2 - k^2} \tag{10}$$

In the same plane, we have the minimum value of the coordinate along the u axis:

$$u_{\min} = 0$$

In the plane of a circle with radius R (the plane that is parallel to $y0_1x_1$ and contains the x_2 axis)—the coordinates on the v axis are:

$$v_{max} = \sqrt{R^2 - \left(k - \frac{P}{2}tan\lambda\right)^2} \tag{11}$$

where

according to the Formula (3) $k = rsin\gamma$

In the same plane, we have the maximum value of the coordinate along the u axis:

$$u_{max} = \frac{P}{2cos\lambda} \tag{12}$$

Determining the profile angle of the cutting edge of the cutter (according to the diagram in Figure 18):

$$\varphi_2 = 2arctan\left(\frac{u_{max}}{(v_{max} - v_{min})}\right) \tag{13}$$

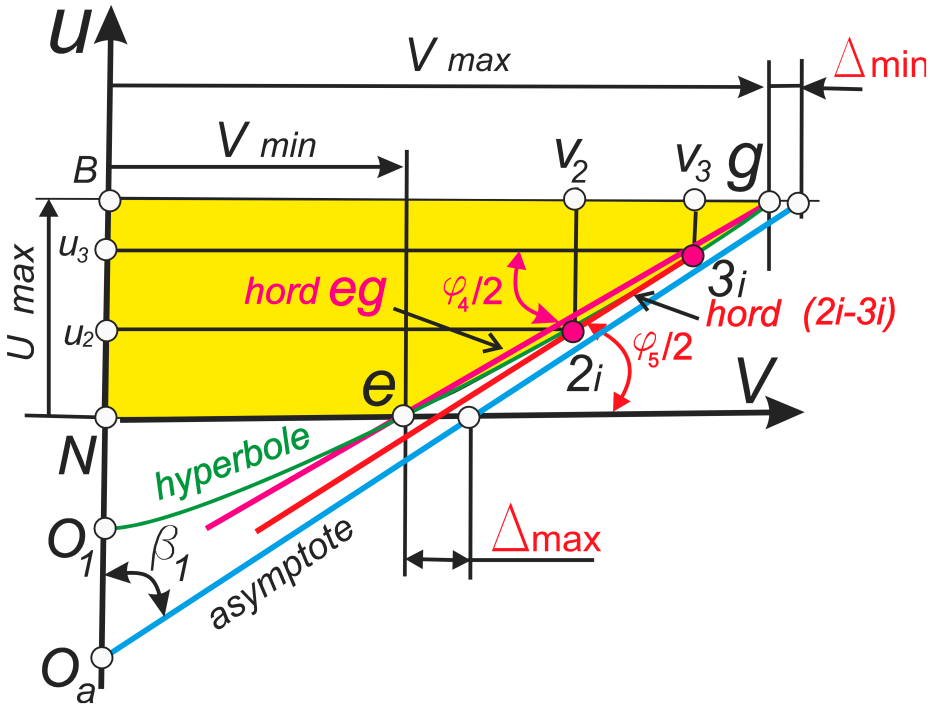

Figure 18. Scheme for determining the profile angle φ_2 of the simulated lateral straight cutting edge of the cutter as a function of its geometric parameters γ and λ.

7. Analytical Study of the Cutting Edge with Geometric Parameters γ and λ

7.1. Derivation of the Cutting-Edge Equation by Solving the System of Equations of a Cone and a Plane

A cone with a half angle at the vertex β in the Cartesian coordinate system XYZ, whose origin is located at the vertex of the cone, is described by the equation:

$$y^2 + z^2 = x^2\tan^2(\beta), \tag{14}$$

The equation of the plane is given by:

$$y = k, \tag{15}$$

The equation of the cutting edge (a hyperbola) is obtained as a solution to the system of Equations (14) and (15):

$$z = \pm\sqrt{x^2\tan^2(\beta) - k^2}. \tag{16}$$

After substituting $\beta = \pi/2 - \varphi/2$ and $k = r\cdot\sin\gamma$, and considering only the "+" sign, can be shown that the right-hand sides of Equations (16) and (7) are identical. Thus, the problem in its alternative formulation has the same solution.

If the plane given by Equation (15) is additionally rotated by an angle λ about the line of intersection of the planes $y = k$ and $x = r\cdot\tan(\varphi/2)$, its equation becomes:

$$\left(-r\cdot tan\left(\frac{\varphi}{2}\right) + x\right)\sin(\lambda) + (-k + y)\cos(\lambda) = 0 \tag{17}$$

The solution of the system of Equations (14) and (17) yields the equation of the intersection curve:

$$z = \pm\sqrt{x^2\tan^2(\beta) - \left(r\cdot tan\left(\frac{\varphi}{2}\right)\tan(\lambda) + k - x\tan(\lambda)\right)^2}, \tag{18}$$

where $r = d_2/2 - H/2$,

H—height of the fundamental triangle, d_2—pitch diameter.

After substituting $\beta = \pi/2 - \varphi/2$ and $k = r\cdot\sin\gamma$, and considering only the "+" sign, the final equation of the hyperbola in the plane containing the cutting edge is obtained:

$$y = \sqrt{x^2cot^2(\varphi) - \left(r\cdot tan\left(\frac{\varphi}{2}\right)\cdot\tan(\lambda) + r\cdot sin(\gamma) - x\cdot\tan(\lambda)\right)^2} \tag{19}$$

7.2. The Angle of Inclination of the Chord (2i-3i) (Figure 18) to the Thread Axis

Segment (2i–3i) (red points) is linear interpolation of a hyperbola within the cutting-edge points 2–3 of the cutter. The endpoints of the segment have coordinates (u_2, v_2) and (u_3, v_3). According to Figure 17, the coordinate values are given as: $u_2 = |Nu_2| = |x_2 - x_c|/\cos\lambda$, $u_3 = |Nu_3| = |x_3 - x_c|/\cos\lambda$. Since the angle λ does not exceed 7°, and therefore $\cos\lambda > 0.99$, it can be assumed that the coordinates $u_2 = x_2$, $u_3 = x_3$. The coordinates v_2 and v_3 are determined using Formula (20) from the values of the arguments u_2 and u_3.

$$\frac{\varphi_5}{2} = arctan\left(\frac{x_3 - x_2}{y_{3i} - y_{2i}}\right) \tag{20}$$

where the values of y_{3i} and y_{2i} are obtained from Equation (19) using the values of x_3 and x_2.

7.3. Maximum and Minimum Deviation of the Theoretical Fundamental Triangle

According to Figure 11 and Formulas (8) and (9), it is shown that the hyperbolic curve has the smallest deviation Δmin from the asymptote in the plane of the large base of the cone (radius R), while the largest deviation Δmax occurs in the plane of the small base (radius r). To account the influence of the inclination angle λ on these values, the following expressions are used:

$$\Delta_{max} = y_c - y_e, \tag{21}$$

$$\Delta_{min} = y_p - y_g, \tag{22}$$

where y_c and y_p are determined from Figures 2–4, Tables 7–9, and ye and yg are calculated using Formula (19), provided that the arguments x_c, x_p are determined based on Figures 2–4 and Tables 7–9.

Table 7. Summary of geometric and design data for trapezoidal threads with a nominal diameter of 24 mm and a pitch of 8 mm according to ISO 2904 [73] and GOST 9484-81 [71] (Figure 3).

Symbol	Parameter Name	Formula	Value
Data according to standards			
d	Major diameter		25.00mm
d_2	Pitch diameter		20 mm
P	Pitch		8 mm
d_3	Minor diameter		15.00 mm
H	Height of the fundamental triangle	$H = 1.866P$	14.928 mm
H_1	Height of the profile	$H_1 = 0.5\ P$	7.464 mm
a_c	Clearance		0.5 mm
h_3	External thread profile height	$h_3 = H_1 + a_c$	4.5 mm
Calculated data			
R	Major radius of the guide cone	$R = d_2/2 + H/2$	17.464 mm
r	Minor radius of the guide cone	$r = d_2/2 - H/2$	2.536 mm
Formulas for calculating the profile angle of the cutting edge φ2			
$X2$	X-coordinate of point 2	$X2 = (r + (H - h_3)/2)\tan(\varphi/2)$,	2.077 mm
$X3$	X-coordinate of point 3	$X3 = (r + (H + h_3)/2)\ \tan(\varphi/2)$,	3.283 mm
$Y2$	Y-coordinate of point 2	$Y2 = r + (H - h_3)/2$	7.75 mm
$Y3$	Y-coordinate of point 3	$Y3 = r + (H + h_3)/2$	12.25 mm
Formulas for calculating the guide cone			
Yc	Y-coordinate of point C	$Yc = r$	2.536 mm
Yp	Y-coordinate of point P	$Yp = R$	17.464 mm
Xc	X-coordinate of point C	$Xc = r\tan(\varphi/2)$	0.679 mm
Xp	X-coordinate of point P	$Xp = R\tan(\varphi/2)$	4.679 mm

Table 8. Results of calculation of the extreme points e and g of the hyperbola obtained within the initial theoretical triangle of a trapezoidal thread with a nominal diameter of 24 mm and a pitch of 8 mm during modeling of turning with a cutter having geometric parameters λ = 7°, γ = 10°.

Coordinates x	By Formula (19)	According to the Formulas (10) and (11)
Xp = 4.679 mm	yg = 17.462 mm	$Vmax$ = 17.464 mm
Xc = 0.679 mm	ye = 2.495 mm	$Vmin$ = 2.497 mm

Table 9. Results of calculation of cutter profile data for turning trapezoidal threads with a nominal diameter of 24 mm and a pitch of 8 mm according to the ISO 2904.

N	Rake Angle γ, °	Inclination Angle λ, °	Profile Angle of the Cutter $\varphi_5/2$, °	Deviation |ce| Δmax, μm	Deviation |pg| Δmin, μm
1	10	7	14.99	39	0
2	4	7	15.00	6	3
3	0	7	15.01	≈0	7
4	0	0	15.00	0	0

8. Results of Calculation and Modeling of the Interpolated Hyperbolic Profile of the Cutting Edge of the Cutter with a Non-Zero Value of the Rake Angle and the Angle of Inclination of the Cutting Edge

8.1. Cutter with Geometric Parameters $\lambda \neq 0$, $\gamma \neq 0$ for Turning Trapezoidal Threads with a Nominal Diameter of 24 mm and a Pitch of 8 mm ($\varphi = 30°$) According to the Standard ISO 2904 [73] and GOST9484-81 [71]

Since the pitch diameter is $d_2 = 20$ mm and the pitch is 8 mm (Table 7), the thread lead angle is $\psi = 7.3°$. The cutting-edge rake angle is taken as $\lambda = 7°$ (Figure 19).

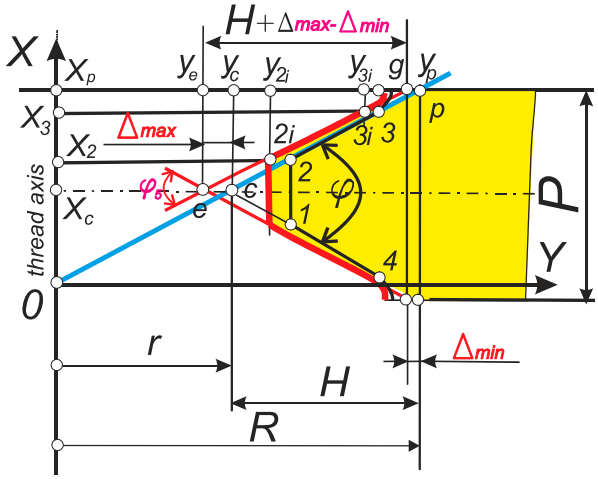

Figure 19. Model of the cutting edge of the cutter for turning trapezoidal threads according to standards [71–73].

8.1.1. Results of Calculation of the Position of the Extreme Points of the Hyperbolic Profile of the Cutter for Turning Trapezoidal Threads with a Nominal Diameter of 24 mm and a Pitch of 8 mm According to ISO 2904 [73] and GOST9484-81 [71]

The results of calculating the positions of points e and g based on their coordinates x_c and x_p (Table 8) indicate the identity of the calculated coordinates y_g and y_e, obtained using Formula (19). These values are derived using the method of solving the system of equations describing the surfaces of the cone and the translated and rotated plane presented in Section 7. They also correspond to the values of Vmax and Vmin according to Formulas (10) and (11) (Figure 18), obtained using the interpolation method based on the two extreme points of the hyperbolic profile described in Section 6.

8.1.2. Results of Calculation of Cutter Profile Elements for Turning Trapezoidal Threads with a Nominal Diameter of 24 mm and a Pitch of 8 mm According to ISO 2904 [75] and GOST 9484-81 [73]

Based on Formulas (19)–(22) and the calculated values in Table 7, the profile elements of the cutter for turning trapezoidal threads with a nominal diameter of 24 mm and a pitch of 8 mm were obtained for the parameter values $\lambda = 7°, 0°$ and $\gamma = 10°, 4°, 0°$ (Table 9).

8.2. Cutter with Geometric Parameters $\lambda \neq 0$, $\gamma \neq 0$ for Turning Tapered NC10 Tool-Joint Threads According to API 7 Standard [69] form V-0.05

For this thread, the helix angle at the largest diameter is 2.86°. Therefore, the cutting-edge inclination angle is approximately $\lambda \approx 3°$. The profile angle is $\varphi = 60°$. In the first turn of the nipple, the diameters are maximal; if these are taken as the basis for calculations, then according to Figure 2, $R = Rt$ and $r = rt$ (Figure 20).

Based on Formulas (19)–(22) and the calculated values in Table 10, the results of the cutter profile elements for tapered NC10 tool-joint thread according to API 7 standard are obtained for the parameter values: $\lambda = 3°, 0°$ and $\gamma = 10°, 4°, 0°$ (Table 11).

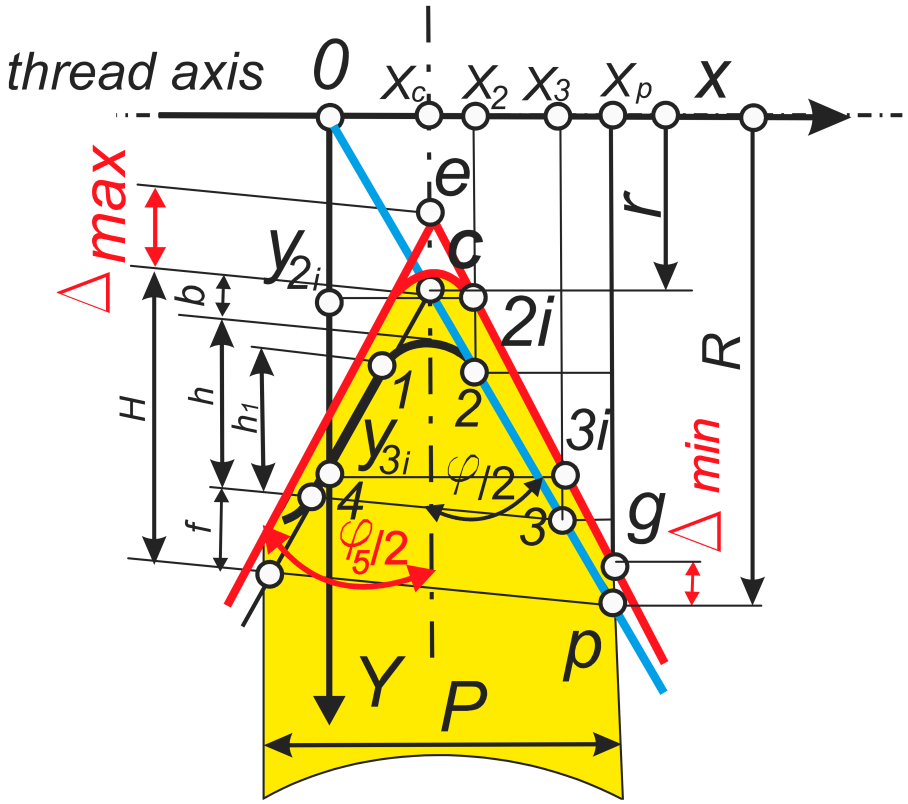

Figure 20. Cutting edge model of a tool for turning API 7 Standard tool-joint threads.

Table 10. Summary of geometric and design data for tapered NC10 tool-joint thread according to API 7 [69] form V-0.05.

Symbol	Parameter Name	Formula	Value
	Data according to standards		
d_{2t}	Maximum thread pitch diameter		27 mm
P	Pitch		4.233
H	Height of the fundamental triangle		3.660
b	Height of the profile		1.209 mm
f	Clearance at the crest		1.081 mm
h	Height of external thread profile		1.420 mm
h_1	External thread profile height		1.242 mm
	Calculated data		
R	Larger radius of the guide cone	$R = d_{2t}/2 + H/2$	15.33 mm
r	Smaller radius of the guide cone	$r = dt_2/2 - H/2$	11.67 mm
	Formulas for calculating the profile angle of the cutting edge φ_2		
X_2	X-coordinate of point 2	$X_2 = (r + f)/2) \tan(\varphi/2)$,	7.362 mm
X_3	X-coordinate of point 3	$X_3 = (R - f)/2) \tan(\varphi/2)$,	8.227 mm
Y_2	Y-coordinate of point 2	$Y_2 = r + f$	12.751 mm
Y_3	Y-coordinate of point 3	$Y_3 = R - f$	14.249 mm
	Formulas for calculating the guide cone		
Y_c	Y-coordinate of point C	$Y_c = r$	11.67 mm
Y_p	Y-coordinate of point P	$Y_p = R$	15.33 mm
X_c	X-coordinate of point C	$X_c = rtan(\varphi/2)$	6.74 mm
X_p	X-coordinate of point Z	$X_p = Rtan(\varphi/2)$	8.85 mm

Table 11. Results of calculation of profile data of the cutter for turning tapered tool-joint threads, API standard 7 [69], Form V-0.05 (maximum pitch diameter *D*p =27 mm, profile angle $\varphi = 60°$).

N	Rake Angle γ, °	Inclination Angle λ, °	Profile Angle of the Cutter $\varphi_5/2$, °	Deviation Δmax, μm	Deviation Δmin, μm
1	10	3	29.91	149	121
2	4	3	30.00	28	17
3	0	3	29.99	0	1
4	0	0	30.00	0	0

8.3. Cutter with Geometric Parameters $\lambda \neq 0$, $\gamma \neq 0$ for Turning Buttress Threads 7°/45° with Basic Height of 0.6 Pitches (Basic Effective Diameter d = 1.5 × 25.4 = 38.1 mm and Pitch 0.25′ × 25.4 = 6.35 mm, at Which the Thread Lead Angle is $\psi = 3.04°$ ($\lambda = 3°$)

Based on Formulas (19)–(22) and the calculated values in Table 12, the results of the cutter profile elements of buttress threads 7°/45° with basic height of 0.6 pitches (basic effective diameter d = 1.5 × 25.4 = 38.1 mm and pitch 0.25′ × 25.4 = 6.35 mm) are obtained for the parameter values: λ = 3°, 0° and γ = 10°, 4°, 0° (Figure 21, Table 13).

Table 12. Summary of geometric and design data for 7°/45° buttress threads with a basic height of 0.6 pitches (basic effective diameter $d = 1.5 \times 25.4 = 38.1$ mm and pitch 0.25′ × 25.4 = 6.35 mm).

Symbol	Parameter Name	Formula	Value
Data according to standards			
d_2	Basic effective diameter		1.5′ × 25.4 =38.1mm
P	Pitch		0.25′ × 25.4= 6.35 mm
d	Nominal major diameter	$d = d_2 + h$	40.64
N	Height of sharp-V thread	$0.89064P$	5.656
f	Crest truncation	$0.24532P$	1.558 mm
h	Basic height of thread engagement	$0.4P$	2.54 mm
Calculated data			
R	Larger radius of the guide cone	$R = r + H$	21.858 mm
r	Smaller radius of the guide cone	$r = d/2 - f - h$ 20.32	16.202 mm
Formulas for calculating cutting-edge profile angle φ_2			
X_2	X-coordinate of point 2	$X_2 = Y_2 \tan(\varphi_2) = Y_2$,	17.78 mm
X_3	X-coordinate of point 3	$X_3 = Y_3 \tan(\varphi_2)$, $= Y_3$	20.318 mm
Y_2	Y-coordinate of point 2	$Y_2 = r + f$	17.78 mm
Y_3	Y-coordinate of point 3	$Y_3 = f + h + r$	20.318 mm
Formulas for calculating the guide cone			
Y_c	Y-coordinate of point C	$Y_c = r$	16.202 mm
Y_p	Y-coordinate of point P	$Y_p = R$	21.858 mm
X_c	X-coordinate of point C	$X_c = r\tan(\varphi_2)$	16.202 mm
X_p	X-coordinate of point P	$X_p = R\tan(\varphi_2)$	21.858 mm

Table 13. Results of calculation of cutter profile data for turning buttress threads 7°/45° witha basic height of 0.6 pitches and basic effective diameter 1.5′ (38.1 mm).

N	Rake Angle γ, °	Inclination Angle λ, °	Cutter Profile Angle $\varphi_5/2$, °	Deviation Δmax, μm	Deviation Δmin, μm
1	10	3	44.51	246	165
2	4	3	44.89	40	16
3	0	3	45.01	0	2
4	0	0	45.00	0	0

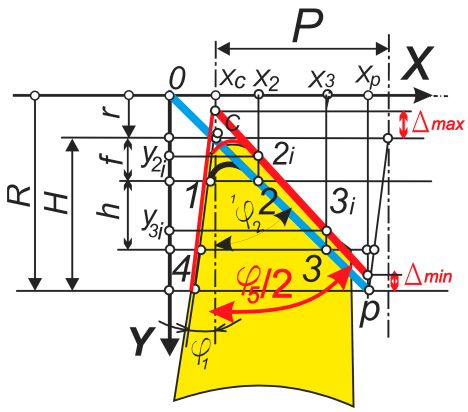

Figure 21. Cutting edge model of a 7°/45° buttress thread-turning tool.

9. Experimental Verification of Analytical Dependencies

9.1. Turning for Threading-like Grooves

Turning was carried out on a lathe model 1A616 (Middle Volga Machine Tool Plant, Samara, USSR). VORGEN Ser 3232 P22 (VORGEN CUTTING TOOLS, Konya, Turkey) cutter tool is used for turning external threads. Carbide threading insert is for manufacturing standard form I tool-joint threads GOST 50864-96 [70] (Figure 22).

Figure 22. Threading cutting tool with two shims: side view and top view of the thread cutting insert.

The lower shim is ordinary. The additional upper shim provides a rake angle of $\gamma = -8°$, which contributes to the tool life. It is made on an electric spark machine Mitsubishi Electric MV12005 (Mitsubishi Electric Corporation, Tokio, Japan) (Figure 23).

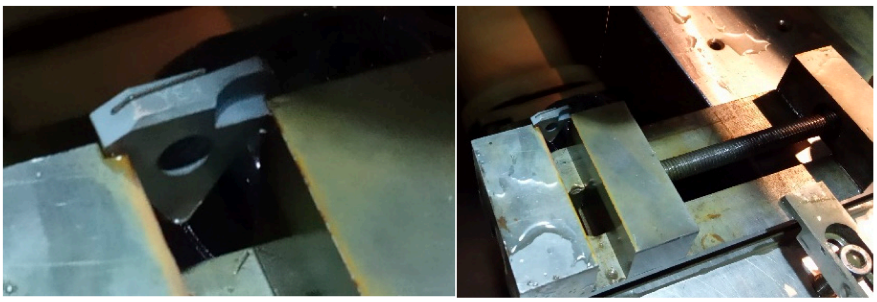

Figure 23. Electro-spark discharge machining of the backing shim.

The workpiece is made of duralumin AlCu4Mg1, 2024 (ISO), diameter—40 mm (Figure 24). Spindle speed is 750 min^{-1}, infeed is 0.16 mm/rev.

Table 14 summarizes the data of the profile of the I-shaped tool-joint thread according to the standard [70]. The input parameters are calculated and the coordinates of the key points of the standard profile are indicated.

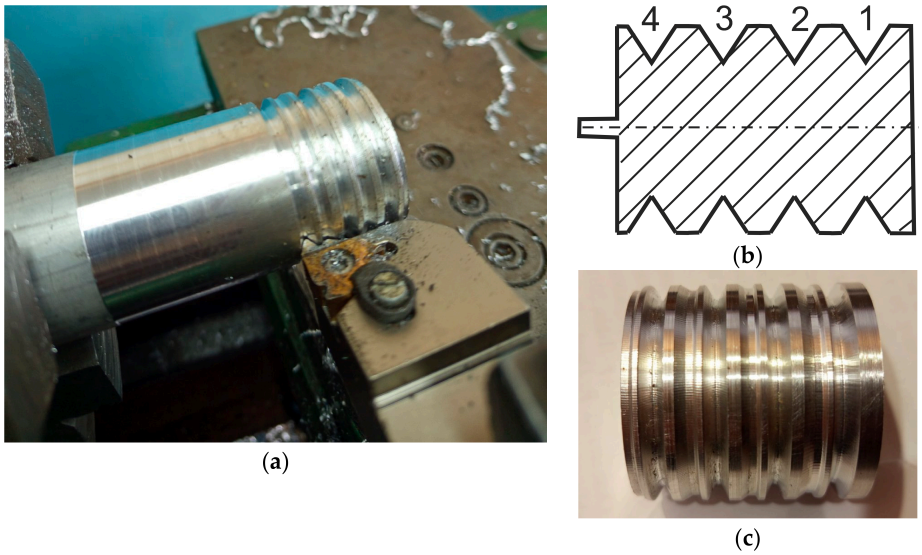

(**a**) (**b**) (**c**)

Figure 24. Preparation of a part with 4 grooves having a threaded profile: (**a**) the process of turning the grooves, (**b**) numbering of the grooves, (**c**) photo of an experimental sample with 4 grooves having a profile I of the tool-joint thread.

Table 14. Summary of geometric and design data for tapered tool-joint thread Z-66 according to GOST 50864-96 [70] (analog to 2 3/8 reg) according to API 7 [69] form V-0.040.

Symbol	Parameter Name	Formula	Value
	Data according to standards		
d_{2t}	Maximum thread pitch diameter		39.25 mm
P	Pitch		5.08
H	Height of the fundamental triangle		4.376
b	Height of the profile		0.875 mm
f	Clearance at the crest		0.508 mm
h	Height of external thread profile		2.993 mm
h_1	External thread profile height		2.626 mm
	Calculated data		
R	Larger radius of the guide cone	$R = d_{2t}/2 + H/2$	21.813 mm
r	Smaller radius of the guide cone	$r = dt_2/2 - H/2$	17.437 mm
	Formulas for calculating the profile angle of the cutting edge φ_2		
X_2	X-coordinate of point 2	$X_2 = (r + f)\tan(\varphi/2)$,	10.354 mm
X_3	X-coordinate of point 3	$X_3 = (R - f)\ \tan(\varphi/2)$,	12.293 mm
Y_2	Y-coordinate of point 2	$Y_2 = r + f$	17.945 mm
Y_3	Y-coordinate of point 3	$Y_3 = R - f$	21.305 mm
	Formulas for calculating the guide cone		
Y_c	Y-coordinate of point C	$Y_c = r$	17.437 mm
Y_p	Y-coordinate of point P	$Y_p = R$	21.813 mm
X_c	X-coordinate of point C	$X_c = rtan(\varphi/2)$	10.061 mm
X_p	X-coordinate of point Z	$X_p = Rtan(\varphi/2)$	12.586 mm

9.2. Groove Profile Study

The study was conducted using an optical microscope PMT-3 (Leningrad Optical-Mechanical Association, Leningrad, USSR) and a camera attachment (magnification × 200) (Figure 25). A laboratorian part for providing an axial profile is divided into two equal parts on a Mitsubishi Electric MV12005 electric spark machine (Figure 25). A wire with a diameter of 0.2 ± 0.01 mm was used for this.

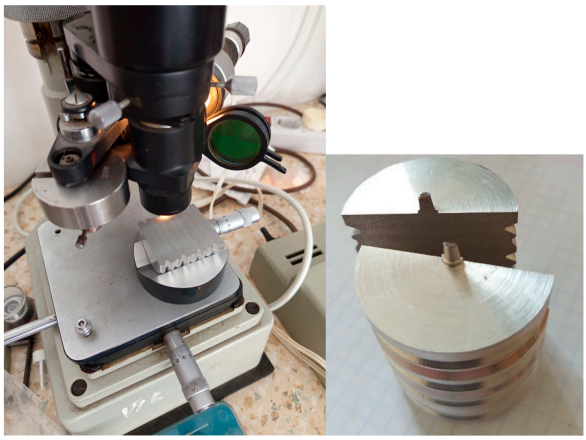

Figure 25. A part divided in half along the axis is mounted in a prism on a microscope stand.

A laboratory detail divided in half along the axis is mounted in a prism on a microscope stand.

9.3. Analysis of the Experiment Results

Cross-section photographs were taken using an optical microscope. OpenCV functions were used to select pixels of the profile edges. First, the image was blurred using a Gaussian filter (GaussianBlur function with a smoothing kernel size of k size = 5). Then, edges were searched using the Canny algorithm (Canny function with parameters threshold1 = 20, threshold2 = 20). Additionally, manual image cleaning from noise was used.

The pixels of the left and right sides of the profile were approximated by linear approximation (y = slope*x + intercept) using the least squares method. The slope values were used to obtain the angles of inclination to the X axis. The thread profile angle φ_e calculated from them is given in Table 15.

Table 15. Experimental results and deviations from the theoretical value $\varphi_t = 59.615°$.

Pos.	φ_e, °	$\varphi_e - \varphi_t$, °	Ra (Left), µm	Ra (Right), µm
1	59.722	0.107	6.8	4.2
2	59.843	0.228	5.8	4.8
3	59.547	−0.068	4	5.3
4	59.701	0.086	6.6	4.3
mean	59.703	0.088	5.8	4.65
std	0.121	0.121	1.275	0.507

The roughness of the profile Ra (left and right sides) was measured from the image by converting y = y-intercept, rotating by the arctan(slope) angle and scaling the pixels in millimeters (Table 15).

Based on the initial data from Table 14 and Formula (19), the theoretical value $\varphi t = 59.615°$ of the profile angle was obtained.

The average value of φ_e deviates from the theoretical value by 0.088°. Since the accuracy of the angle of the tool-joint thread profile is ±0.67°, the width of the scattering field of φ_e values (6*std) is approximately half of the tolerance field. The maximum deviation from the theoretical value (0.228°) is 34% of the tolerance.

10. Discussions

The data in Table 6 (8) indicate that the simulated cutting edge has a technologically insignificant convexity of 0.002 mm at the rake angle of $\gamma = 20°$, and a convexity of 0.00056 mm at the rake angle of $\gamma = 10°$, which is practically impossible to reproduce. Taking

these data into account, as well as recommendations for the rake angles range from 0 to 15°, the authors consider it advisable to replace the curvilinear profile of the cutting edge with a straight line passing through the two extreme points. This forms the basis for linear interpolation between the two extreme points of the hyperbolic cutting-edge profile as a function of both the rake angle at the nose and its inclination angle of the cutting edge, i.e., using Formulas (19) and (20). Expressions (10) and (11) present a visually clear and concise method for calculating the coordinates of the extreme points of the theoretical cutting-edge profile, which is intended for a thread cutter with non-zero values of the rake angle γ and the inclination angle λ.

Equation (7) is the result of deriving the hyperbolic profile function of a thread cutter from the thread parameters and the value of rake angle γ. This derivation is as geometrically transparent as possible and theoretically accurate, as it is based on the methods of descriptive geometry and trigonometry.

Formula (19) is obtained using an analytical method for solving the problem of the intersection of a cone with a cutting-edge plane that has been translated and rotated. This analytical approach is the most general and allows one to easily obtain the hyperbolic profile function as a function of the parameters γ and λ. If $\lambda = 0$, then Formula (19) is transformed into Formula (7). Equation (19) also confirms the results obtained from expressions (10) and (11).

The authors' proposed simplified approach for determining the coordinates of points on the threaded profile, using the relations $u_2 = x_2$, $u_3 = x_3$ in Section 7.2 is debatable. Alternative expressions are also given: $u_2 = |Nu_2| = |x_2|/\cos\lambda$ and $u_3 = |Nu_3| = |x_3|/\cos\lambda$. However, these expressions are not theoretically accurate since the coordinate origin O and the point Oλ about which the UV plane is rotated do not coincide. The calculation of the values Δmax and Δmin, according to the authors, is important not for analyzing the cutting-edge profile itself, but for determining the maximum radial feed of the cutter. In fact, the radial feed should be increased by the value $(\Delta\max - \Delta\min)\cdot\cos\gamma$.

To use cutters with a non-zero λ value, it is sufficient to install a suitable shim with an angle of λ, supplied by the manufacturer. To ensure a non-zero γ angle, the cutter holder can be adjusted, for example, by milling its support surface at an angle equal to γ.

The experimental results are indicative, because the analysis does not take into account machining and measurement errors. The profile roughness Ra and its measurement errors as random variables also affect the measurement accuracy of φ_e (Figure 26).

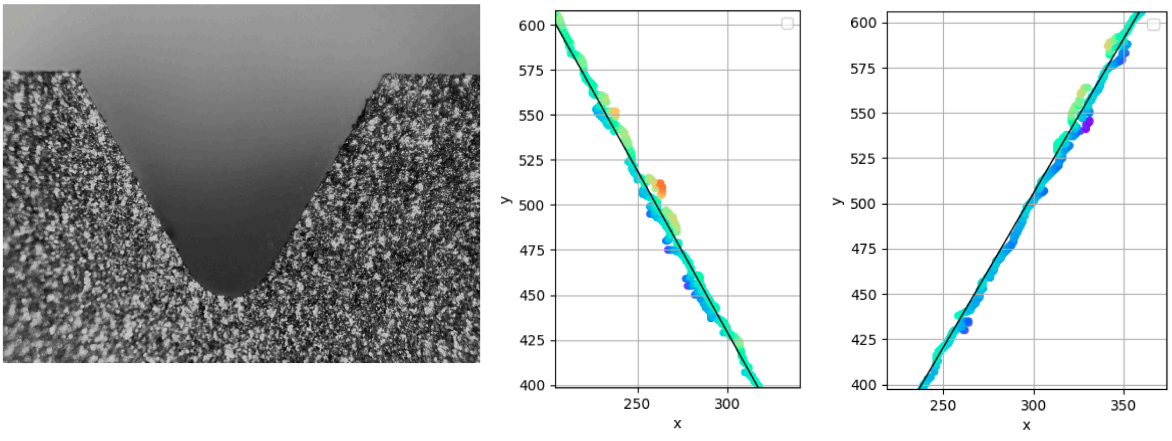

(**a**) (**b**) (**c**)

Figure 26. Profile of groove No. 3 (**a**) and parts of the bitmap images of the left (**b**) and right (**c**) sides of the profile, approximated by straight lines (1 mm = 470 pixels). The color shows the deviation from the line.

11. Conclusions

1. Turning cutters used for manufacturing threaded parts from difficult-to-machine materials, especially parts with a large pitch (such as oil and gas threads with triangular and buttress profiles, and jack screws and lead screws with trapezoidal threads), require non-zero values of the rake angle γ and the cutting-edge inclination angle λ to ensure tool life. This necessitates analytical approaches to solving the problem of profiling the geometry of a high-precision cutting-edge, which consists of the following:

    1.1 Profile modeling is based on functions whose arguments are:

    - geometric parameters of the thread (diameter, pitch, and thread profile angle);
    - geometric parameters of the cutter (rake angle and cutting-edge inclination angle).

    1.2 Theoretically, these functions, using several analytical approaches, describe the hyperbolic curve of the profile as the intersection of the guiding thread cone and the plane containing the cutting edge. The results obtained using two approaches (descriptive geometry with trigonometric derivation and analytical geometry) are identical.

    1.3 Theoretically, it is reasonable to replace the curvilinear hyperbolic profile of the cutting edge with a rectilinear one, in particular by interpolating it between the two extreme points of the thread profile. The feasibility of this replacement is confirmed by calculating the hyperbola concavity, which does not exceed 2 μm relative to the interpolated chord.

    1.4 In the case of turning large-pitch threads, especially with small diameters, there is a technological need to significantly increase the cutting-edge inclination angle. However, there is no need to significantly change the thread profile angle φ, which is confirmed by calculation examples for three different types of threads: tool-joint, trapezoidal and buttress.

2. For the calculation examples of the profile angle φ, cutter models with maximum cutting-edge inclination angles ranging from $\lambda = 7^\circ$ (for trapezoidal threads) down to $\lambda = 3^\circ$ (for tool-joint threads and buttress threads) were adopted. For the same groups of cutters, different rake angles values γ were considered: 10°, 4°, and 0°. This regulates their application for manufacturing threads on parts made of materials with different machinability. The calculations show the following:

    2.1 The smallest deviations in profile angles were observed in cutters models with trapezoidal threads. These models demonstrated the highest theoretical accuracy of the cutting-edge profile $\varphi/2 = 15^\circ \pm 0.01^\circ$, for all values of λ and γ. This is attributed to the small value of the thread profile angle $\varphi/2$, as well as the relatively large tolerance ($25' \approx 0.42^\circ$) (Table 1). This also confirms the possibility of using conventional carbide inserts for cutters with $\gamma < 10^\circ$ and $\lambda < 7^\circ$.

    2.2 The results of the calculation for cutters used in turning tapered tool-joint threads showed satisfactory accuracy of the cutting-edge profile for $\lambda = 4^\circ$, $\lambda = 3^\circ$, and lower values. Under the condition of $\lambda = 3^\circ$ and $\gamma = 10^\circ$, the calculated value of the flank angle $\varphi/2$ is 29.91 °, i.e., the deviation is 0.09°. According to the standard, the tolerance $\varphi/2$ is $\pm 40'$, or approximately $\pm 0.7^\circ$. Therefore, it can be stated that the use of a conventional cutting insert with a profile $\varphi/2 = 30^\circ$ and parameters $\lambda = 3^\circ$ and $\gamma = 10^\circ$ or lower is suitable.

2.3 The use of non-zero rake angles for cutters used in buttress threads can significantly increase the deviation of the profile angle due to its large value ($\varphi = 45°$). The deviation is 0.11° at $\gamma = 4°$ and 0.49° at $\gamma = 10°$ (Table 13). According to the standard (Table 3), these deviations should not exceed $4' \approx 0.067$ °. Therefore, it can be stated that the use of a conventional cutting insert with a buttress profile of 45°/7° with parameters $\lambda = 3°$ and $\gamma = 10°$ is unsuitable for thread diameters not exceeding 1.5 inches (38 mm).

Experimental verification on a lathe confirms the theoretical results.

In the future, the authors plan to expand this study by investigating the influence of tangential displacement of the cutting-edge profile relative to the thread axis on its function.

Author Contributions: Conceptualization, C.B., O.O. and V.K.; methodology, C.B. and O.O.; software, O.O. and V.K.; validation, V.K., Y.K. and S.B.; formal analysis, O.O. and Y.K.; investigation, C.B. and O.O.; resources, L.S. and Y.K.; data curation, L.S. and S.B.; writing—original draft preparation, O.O. and V.K.; writing—review and editing, P.D., V.K. and S.B.; visualization, Y.K. and P.D.; supervision, L.S. and P.D.; project administration, O.O.; funding acquisition, O.O. All authors have read and agreed to the published version of the manuscript.

Funding: This research was funded by the Ministry of Education and Science of Ukraine, grant number PK 0124U000654.

Data Availability Statement: Data are contained within the article.

Conflicts of Interest: The authors declare no conflicts of interest.

References

1. Nascimento, A.; Mantegazini, D.Z.; Mathias, M.H.; Reich, M.; Hunt, J.D. O&G, Geothermal Systems, and Natural Hydrogen Well Drilling: Market Analysis and Review. *Energies* **2025**, *18*, 1608. [CrossRef]
2. Sharmin, T.; Rodoshi Khan, N.; Akram, M.S.; Ehsan, M. A State-of-the-Art Review on Geothermal Energy Extraction, Utilization, and Improvement Strategies: Conventional, Hybridized, and Enhanced Geothermal Systems. *Int. J. Thermofluids* **2023**, *18*, 100323. [CrossRef]
3. Matiyiv, K.; Klymchuk, I.; Arkhypova, L.; Korchemlyuk, M. Surface water quality of the prut river basin in a tourist destination. *Ecol. Eng. Environ. Technol.* **2022**, *23*, 107–114. [CrossRef]
4. Kravchynskyi, R.L.; Khilchevskyi, V.K.; Korchemluk, M.V.; Arkhypova, L.M.; Plichko, L.V. Criteria for identification of landslides in the upper Prut River basin on satellite images. *Geoinformatics* **2021**, *2021*, 1–6. [CrossRef]
5. Prykhodko, M.; Arkhypova, L.; Fomenko, N.; Syrovets, S.; Varianichko, V.; Osypov, D. Economic value of ecosystem services in the landscapes of Ukraine. In *Proceedings of the 17th International Conference Monitoring of Geological Processes and Ecological Condition of the Environment, Kyiv, Ukraine, 7–10 November 2023*; EAGE: Aberdeen, UK, 2023; pp. 1–5. [CrossRef]
6. Glibovytska, N.; Rashevska, H.; Arkhypova, L.; Adamenko, Y.; Orfanova, M. Impact of electric power facilities on natural phytocenotic diversity. *Ukr. J. For. Wood Sci.* **2024**, *15*, 8–22. [CrossRef]
7. Wu, B.; Zhang, K.; Meng, G.; Suo, X. Optimization of Recharge Schemes for Deep Excavation in the Confined Water-Rich Stratum. *Sustainability* **2023**, *15*, 5432. [CrossRef]
8. Vlasiy, O.; Mazurenko, V.; Ropyak, L.; Rogal, O. Improving the aluminum drill pipes stability by optimizing the shape of protector thickening. *East.-Eur. J. Enterp. Technol.* **2017**, *1*, 25–31. [CrossRef]
9. Qin, J.; Feng, Z.; Wang, M.; Gong, H.-X.; Mei, X.-Z.; Yang, H.-Y. Research on the design and performance of drill pipe joints based on fracture mechanics methods. *Sci. Rep.* **2025**, *15*, 22790. [CrossRef] [PubMed]
10. Kopei, V.; Onysko, O.; Panchuk, V.; Pituley, L.; Schuliar, I. Influence of Working Height of a Thread Profile on Quality Indicators of the Drill-String Tool-Joint. In *Advanced Manufacturing Processes III, 3rd Grabchenko's International Conference on Advanced Manufacturing Processes (InterPartner-2021), Odessa, Ukraine, 7–10 September 2021*; Springer: Cham, Switzerland, 2022; pp. 395–404. [CrossRef]
11. Prysyazhnyuk, P.; Molenda, M.; Romanyshyn, T.; Ropyak, L.; Romanyshyn, L.; Vytvytskyi, V. Development of a hardbanding material for drill pipes based on high-manganese steel reinforced with complex carbides. *Acta Montan. Slovaca* **2022**, *27*, 685–696. [CrossRef]

12. Kopei, V.; Onysko, O.; Odosii, Z.; Pituley, L.; Goroshko, A. Investigation of the influence of tapered thread profile accuracy on the mechanical stress, fatigue safety factor and contact pressure. In *New Technologies, Development and Application IV, Proceedings of the NT 2021, Sarajevo, Bosnia and Herzegovina, 23–25 June 2022*; Karabegović, I., Ed.; Lecture Notes in Networks and Systems; Springer: Cham, Switzerland, 2021; Volume 233, pp. 177–185. [CrossRef]
13. Shatskyi, I.; Ropyak, L.; Velychkovych, A. Model of contact interaction in threaded joint equipped with spring-loaded collet. *Eng. Solid Mech.* **2020**, *8*, 301–312. [CrossRef]
14. Croccolo, D.; De Agostinis, M.; Fini, S.; Mele, M.; Olmi, G.; Scapecchi, C.; Tariq, M.H.B. Failure of Threaded Connections: A Literature Review. *Machines* **2023**, *11*, 212. [CrossRef]
15. Ropyak, L.Y.; Vytvytskyi, V.S.; Velychkovych, A.S.; Pryhorovska, T.O.; Shovkoplias, M.V. Study on grinding mode effect on external conical thread quality. *IOP Conf. Ser. Mater. Sci. Eng.* **2021**, *1018*, 012014. [CrossRef]
16. Chudyk, I.; Raiter, P.; Grydzhuk, Y.; Yurych, L. Mathematical model of oscillations of a drill tool with a drill bit of cutting-scraping type. *Nauk. Visnyk Natsionalnoho Hirnychoho Univer.* **2020**, *1*, 52–57. [CrossRef]
17. Akl, W.; Alsupie, H.; Sassi, S.; Baz, A.M. Vibration of Periodic Drill-Strings with Local Sources of Resonance. *Vibration* **2021**, *4*, 586–601. [CrossRef]
18. Landar, S.; Velychkovych, A.; Ropyak, L.; Andrusyak, A. A Method for Applying the Use of a Smart 4 Controller for the Assessment of Drill String Bottom-Part Vibrations and Shock Loads. *Vibration* **2024**, *7*, 802–828. [CrossRef]
19. Liu, W.; Yang, F.; Zhu, X.; Chen, X. Stick-slip vibration behaviors of BHA and its control method in highly- deviated wells. *Alex. Eng. J.* **2022**, *61*, 9757–9767. [CrossRef]
20. Bembenek, M.; Grydzhuk, Y.; Gajdzik, B.; Ropyak, L.; Pashechko, M.; Slabyi, O.; Al-Tanakchi, A.; Pryhorovska, T. An Analytical–Numerical Model for Determining "Drill String–Wellbore" Frictional Interaction Forces. *Energies* **2024**, *17*, 301. [CrossRef]
21. Velichkovich, A.S.; Popadyuk, I.I.; Shopa, V.M. Experimental study of shell flexible component for drilling vibration damping devices. *Chem. Pet. Eng.* **2011**, *46*, 518–524. [CrossRef]
22. Li, F.P. Surface Galling Mechanism Analysis of Rotary Shouldered Thread Connection. *Mater. Sci. Forum* **2020**, *993*, 1286–1292. [CrossRef]
23. Velychkovych, A.; Mykhailiuk, V.; Andrusyak, A. Numerical Model for Studying the Properties of a New Friction Damper Developed Based on the Shell with a Helical Cut. *Appl. Mech.* **2025**, *6*, 1. [CrossRef]
24. Landar, S.; Velychkovych, A.; Mykhailiuk, V. Numerical and analytical models of the mechanism of torque and axial load transmission in a shock absorber for drilling oil, gas and geothermal wells. *Eng. Solid Mech.* **2024**, *12*, 207–220. [CrossRef]
25. Shatskyi, I.; Velychkovych, A. Analytical Model of Structural Damping in Friction Module of Shell Shock Absorber Connected to Spring. *Shock Vib.* **2023**, *2023*, 4140583. [CrossRef]
26. Velychkovych, A.; Petryk, I.; Ropyak, L. Analytical study of operational properties of a plate shock absorber of a sucker-rod string. *Shock Vib.* **2020**, *1*, 3292713. [CrossRef]
27. Zheng, Y.; Zhang, Y.; Sun, B.; Zhang, B.; Zhang, S.; Jin, S.; Xiao, Z.; Chu, S.; Jing, Y.; Zhang, Z. Corrosion Behavior and Mechanical Performance of Drill Pipe Steel in a CO_2/H_2 S-Drilling-Fluid Environment. *Processes* **2024**, *12*, 502. [CrossRef]
28. Li, L.; Lian, Z.; Zhou, C. Failure Analysis of Drill Pipe during Working Process in a Deep Well: A Case Study. *Processes* **2022**, *10*, 1765. [CrossRef]
29. Wang, Y.; Qian, C.; Kong, L.; Zhou, Q.; Gong, J. Design Optimization for the Thin-Walled Joint Thread of a Coring Tool Used for Deep Boreholes. *Appl. Sci.* **2020**, *10*, 2669. [CrossRef]
30. Pryhorovska, T.O.; Ropyak, L. Machining Error Influnce on Stress State of Conical Thread Joint Details. In *Proceedings of the 2019 IEEE 8th International Conference on Advanced Optoelectronics and Lasers (CAOL) 2019, Sozopol, Bulgaria, 6–8 September 2019*; IEEE: New York, NY, USA, 2019; pp. 493–497. [CrossRef]
31. Tutko, T.; Dubei, O.; Ropyak, L.; Vytvytskyi, V. Determination of Radial Displacement Coefficient for Designing of Thread Joint of Thin-Walled Shells. In *Advances in Design, Simulation and Manufacturing IV, Proceedings of the 4th International Conference on Design, Simulation, Manufacturing: The Innovation Exchange, DSMIE 2021, Lviv, Ukraine, 8–11 June 2021*; Lecture Notes in Mechanical Engineering; Springer: Cham, Switzerland, 2021; pp. 153–162. [CrossRef]
32. Kim, B.; Yoon, J.-Y. Structural Optimization of a Circular Symmetric Threaded Connection System Based on the Effect of the Upper Stabbing Flank Corner Radius. *Symmetry* **2022**, *14*, 2553. [CrossRef]
33. Shats'kyi, I.P. Closure of a longitudinal crack in a shallow cylindrical shell in bending. *Mater. Sci.* **2005**, *41*, 186–191. [CrossRef]
34. Shats'kyi, I.P.; Makoviichuk, M.V. Analysis of the limiting state of cylindrical shells with cracks with regard for the contact of crack lips. *Strength Mater.* **2009**, *41*, 560–565. [CrossRef]
35. Zhang, J.-Y.; Peng, C.; Fu, J.-H.; Cao, Q.; Su, Y.; Pang, J.-Y.; Yu, Z.-Q. Analysis of mechanical strengths of extreme line casing joint considering geometric, material, and contact nonlinearities. *Pet. Sci.* **2024**, *21*, 1992–2004. [CrossRef]
36. Shats'kyi, I.P.; Makoviichuk, M.V. Contact interaction of crack lips in shallow shells in bending with tension. *Mater. Sci.* **2005**, *41*, 486–494. [CrossRef]

37. Shatskii, I.P.; Makoviichuk, N.V. Effect of closure of collinear cracks on the stress-strain state and the limiting equilibrium of bent shallow shells. *J. Appl. Mech. Tech. Phys.* **2011**, *52*, 464–470. [CrossRef]
38. Karpus, V.E.; Ivanov, V.A. Locating accuracy of shafts in V-blocks. *Russ. Eng. Res.* **2021**, *32*, 144–150. [CrossRef]
39. Karpus, V.E.; Ivanov, V.A. Choice of the optimal configuration of modular reusable fixtures. *Russ. Eng. Res.* **2012**, *32*, 213–219. [CrossRef]
40. Kusyi, Y.; Onysko, O.; Kuk, A.; Solohub, B.; Kopei, V. Development of the Technique for Designing Rational Routes of the Functional Surfaces Processing of Products. In *New Technologies, Development and Application V, Proceedings of the NT 2022, Sarajevo, Bosnia and Herzegovina, 23–25 June 2022*; Karabegović, I., Ed.; Lecture Notes in Networks and Systems; Springer: Cham, Switzerland, 2022; Volume 472, pp. 135–143. [CrossRef]
41. Kusyi, Y.; Stupnytskyy, V.; Onysko, O.; Dragašius, E. Optimization synthesis of technological parameters during manufacturing of the parts. *Maint. Reliab.* **2022**, *24*, 655–667. [CrossRef]
42. Jasiulewicz-Kaczmarek, M.; Antosz, K.; Zhang, C.; Ivanov, V. Industry 4.0 Technologies for Sustainable Asset Life Cycle Management. *Sustainability* **2023**, *15*, 5833. [CrossRef]
43. Onysko, O.; Panchuk, P.; Kopey, V.B.; Havryliv, Y.; Sculiar, I. Investigation of the influence of the cutter-tool rake angle on the accuracy of the conical helix in the tapered thread machining. *J. Phys. Conf. Ser.* **2021**, *1781*, 012028. [CrossRef]
44. Costa, C.E.; Polli, M.L. Effects of the infeed method on thread turning of AISI 304L stainless steel. *J. Braz. Soc. Mech. Sci. Eng.* **2021**, *43*, 253. [CrossRef]
45. An, Q.L.; Guo, G.G.; Zheng, X.H.; Chen, M.; Liu, G.; Zhang, Y.S. Experimental Study on Cutting Characteristics for Buttress Thread Turning of 13%Cr Stainless Steel. *Key Eng. Mater.* **2010**, *443*, 262–267. [CrossRef]
46. Koleva, S.; Enchev, M.; Szecsi, T. Compensation of the deviations caused by mechanical deformations during machining of threads. *Procedia Manuf.* **2017**, *13*, 480–486. [CrossRef]
47. Li, Z.; Fu, X.; Li, J.; Jiang, B.; Wang, F. Establishment of vibration wear model for turning large-pitch thread tools and its wear suppression method. *Int. J. Adv. Manuf. Technol.* **2020**, *109*, 857–876. [CrossRef]
48. Fu, X.; Li, K.; Li, Z.; Wang, X. A SVM-based design method for cutting edge profile stability of large-pitch thread turning tool considering vibration. *Int. J. Adv. Manuf. Technol.* **2023**, *125*, 4529–4547. [CrossRef]
49. Khani, S.; Shahabi Haghighi, S.; Razfar, M.R.; Farahnakian, M. Improvement of thread turning process using micro-hole textured solid-lubricant embedded tools. *Proc. Inst. Mech. Eng. Part B J. Eng. Manuf.* **2021**, *235*, 1727–1738. [CrossRef]
50. Medvid, I.; Onysko, O.; Panchuk, V.; Pituley, L.; Schuliar, I. Kinematics of the Tapered Thread Machining by Lathe: Analytical Study. In *Advanced Manufacturing Processes II, Proceedings of the 2nd Grabchenko's International Conference on Advanced Manufacturing Processes (InterPartner-2020), Odessa, Ukraine, 8–11 September 2020*; Tonkonogyi, V., Ivanov, V., Trojanowska, J., Oborskyi, G., Grabchenko, A., Pavlenko, I., Edl, M., Kuric, Dasic, P., Eds.; Lecture Notes in Mechanical Engineering; Springer: Cham, Switzerland, 2021; pp. 555–565. [CrossRef]
51. Krawczyk, B.; Szablewski, P.; Mendak, M.; Gapiński, B.; Smak, K.; Legutko, S.; Wieczorowski, M.; Miko, E. Surface Topography Description of Threads Made with Turning on Inconel 718 Shafts. *Materials* **2022**, *16*, 80. [CrossRef]
52. Zawada-Tomkiewicz, A.; Żurawski, Ł.; Tomkiewicz, D.; Szafraniec, F. Sustainability and tool wear of titanium alloy thread cutting in dry and cryogenic conditions. *Int. J. Adv. Manuf. Technol.* **2021**, *114*, 2767–2781. [CrossRef]
53. Slătineanu, L.; Radovanovic, M.; Coteață, M.; Beșliu, I.; Dodun, O.; Coman, I.; Olaru, S.-C. Requirements in designing a device for experimental investigation of threading accuracy. *MATEC Web Conf.* **2017**, *112*, 01005. [CrossRef]
54. Onysko, O.; Kopei, V.; Barz, C.; Kusyi, Y.; Baskutis, S.; Bembenek, M.; Dašić, P.; Panchuk, V. Analytical Model of Tapered Thread Made by Turning from Different Machinability Workpieces. *Machines* **2024**, *12*, 313. [CrossRef]
55. Kopey, V.B.; Onysko, O.R.; Panchuk, V.G. Computerized system based on FreeCAD for geometric simulation of the oil and gas equipment thread turning. *IOP Conf. Ser. Mater. Sci. Eng.* **2019**, *477*, 012032. [CrossRef]
56. Balajti, Z.; Mándy, Z. Proposed solution to eliminate pitch fluctuation in case of conical screw surface machining by apex adjustment. *Procedia Manuf.* **2021**, *55*, 266–273. [CrossRef]
57. Onysko, O.; Kopey, V.; Panchuk, V.; Medvid, I.; Lukan, T. Analitical Study of the kinematic rake angles of the cutting edge of the lathe tool for the tapered thread manufacturing. In *Advanced Manufacturing Processes, Proceedings of the Grabchenko's International Conference on Advanced Manufacturing Processes (InterPartner-2019), Odessa, Ukraine, 10–13 September 2019*; LNME; Springer: Cham, Switzerland, 2020; pp. 236–245. [CrossRef]
58. Máté, M.; Hollanda, D. About the Profile Accuracy of the Involute Gear Hob. *Acta Univ. Sapientiae Electr. Mech. Eng.* **2017**, *9*, 5–18. [CrossRef]
59. Yao, X.; Cui, J.; Yu, H.; Qi, X.; Mi, X.; Jiang, Y.; Wang, M.; Li, X. An improved accuracy-measuring method in manufacturing the lead screw of grating ruling engine. *Precis. Eng.* **2017**, *49*, 344–353. [CrossRef]
60. Prokopiv, V.; Horichok, I.; Mazur, T.; Matkivsky, O.; Turovska, L. Thermoelectric Materials Based on Samples of Microdispersed PbTe and CdTe. In *Proceedings of the 2018 IEEE 8th International Conference Nanomaterials: Application & Properties (NAP), Zatoka, Ukraine, 9–14 September 2018*; IEEE: New York, NY, USA, 2018; pp. 1–4. [CrossRef]

61. Dzundza, B.; Kostyuk, O.; Mazur, T. Software and Hardware Complex for Study of Photoelectric Properties of Semiconductor Structures. In *Proceedings of the 2019 IEEE 39th International Conference on Electronics and Nanotechnology, ELNANO 2019, Kyiv, Ukraine, 16–18 April 2019*; IEEE: New York, NY, USA, 2019; pp. 635–639. [CrossRef]
62. Tolvaly-Roşca, F.; Máté, M.; Forgó, Z.; Pásztor, J. CAD solution to determine points from chipping tool solid model cutting edges. *Műszaki Tudományos Közlemények* **2020**, *12*, 67–70. [CrossRef]
63. Martins, F.S.; Reina-Muñoz, R.; Lira, V.M. System of cutting force data acquisition in mechanical lathes. *DYNA* **2018**, *85*, 16. [CrossRef]
64. Demirpolat, H.; Binali, R.; Patange, A.D.; Pardeshi, S.S.; Gnanasekaran, S. Comparison of Tool Wear, Surface Roughness, Cutting Forces, Tool Tip Temperature, and Chip Shape during Sustainable Turning of Bearing Steel. *Materials* **2023**, *16*, 4408. [CrossRef]
65. Lubis, S.; Rosehan; Darmawan, S.; Indra, B. Tool Wear Analysis of Coated Carbide Tools on Cutting Force in Machining Process of AISI 4140 Steel. *IOP Conf. Ser. Mater. Sci. Eng.* **2020**, *852*, 012083. [CrossRef]
66. Sandvik Coromant. Tread Turning Tools. Available online: https://www.sandvik.coromant.com/en-us/tools/threading-tools/thread-turning-tools (accessed on 28 February 2026).
67. Sun, L.; Cui, X.; Wang, C.; Zhang, Y.; Li, C. Mechanical behavior of material removal under various rake angle diamond tool ultra-precision cutting of titanium alloy. *J. Mater. Res. Technol.* **2025**, *38*, 1302–1312. [CrossRef]
68. Li, A.; Zang, J.; Zhao, J. Effect of cutting parameters and tool rake angle on the chip formation and adiabatic shear characteristics in machining Ti-6Al-4V titanium alloy. *Int. J. Adv. Manuf. Technol.* **2020**, *107*, 3077–3091. [CrossRef]
69. Specification for Threading and Gauging of Rotary Shouldered Thread Connections. ANSI/API SPECIFICATION 7-2 (formerly in SPEC 7). First edition. 2008. Available online: https://www.api.org/ /media/files/publications/addenda-and-errata/exploration-production/7_2_add_1.pdf?la=en (accessed on 15 April 2026).
70. *GOST 50864-96*; Tool-Joint Tapered Thread for Drill String Elements; Profile, Dimensions, Technical Requirements. Federal Agency for Technical Regulation and Metrology: Moscow, Russia, 1997.
71. *GOST 9484–81*; Basic Norms of Interchangeability; Trapezoidal Screw Thread. Profiles. Federal Agency for Technical Regulation and Metrology: Moscow, Russia, 1982.
72. *ASME B1.5-1997 (R2024)*; Acme Screw Threads. ASME: New York, NY, USA, 1997; 124p.
73. *ISO 2904:2020*; ISO Metric Trapezoidal Screw Threads—Basic Dimensions. International Organization for Standardization: Geneva, Switzerland, 2020.
74. *ASME B1.9-1973 (R2025)*; Buttress Inch Screw Threads. ASME: New York, NY, USA, 1973.
75. *API SPEC 5CT-ed.11*; Casing and Tubing. API: Washington, DC, USA, 2023.
76. Walter Tools. Thread Turning. Available online: https://www.walter-tools.com/en-us/products/turning/thread-turning (accessed on 15 April 2026).
77. Workpiece Material Group. Dormer Pramet. Available online: https://www.dormerpramet.com/cz/en/WMG (accessed on 15 April 2026).
78. Ezugwu, E.O.; Okeke, C.I.; Machado, A.R. High speed threading of inclusion-modified steels with coated carbide tools. *J. Mater. Process. Technol.* **1999**, *86*, 216–225. [CrossRef]
79. Pandey, H.D.; Dubey, S.K.D.; Khan, M.Q.; Dubey, O.P. *A Textbook of Analytical Geometry*; Dominant Publishers and Distributors (P) Ltd.: New Delhi, India, 2012; ISBN 978-93-80642-14-7.
80. Privalov, I.I. *Analytical Geometry*; Nauka: Moscow, Russia, 2007; 394p. (In Russian)
81. Shervatov, V.G. *Hyperbolic Functions*; State Publishing House of Technical and Theoretical Literature: Moscow, Russia, 1953; 58p. (In Russian)
82. Kopei, V.; Onysko, O. Threading_dev5.ipynb. Available online: https://colab.research.google.com/drive/1EVUOh9sPqzQxi8Loboyt_3rPYor7AedR (accessed on 15 April 2026).